HHS Public Access

Author manuscript

J Hum Evol. Author manuscript; available in PMC 2021 October 01.

Published in final edited form as:

J Hum Evol. 2020 October ; 147: 102865. doi:10.1016/j.jhevol.2020.102865.

Biomechanics of the mandible of *Macaca mulatta* during the power stroke of mastication: Loading, deformation, and strain regimes and the impact of food type

Olga Panagiotopoulou[a], **Jose Iriarte-Diaz**[b], **Hyab Mehari Abraha**[a], **Andrea B. Taylor**[c], **Simon Wilshin**[d], **Paul C. Dechow**[e], **Callum F. Ross**[f]

[a]Department of Anatomy & Developmental Biology, Monash Biomedicine Discovery Institute, Faculty of Medicine Nursing and Health Sciences, Monash University, Clayton, Melbourne, Victoria 3800, Australia

[b]Department of Biology, University of the South, Sewanee TN 37383 USA

[c]Department of Basic Science, Touro University, California, USA

[d]Comparative Biomedical Sciences, The Royal Veterinary College, Hawkshead Lane, Herts, AL97TA, UK

[e]Department of Biomedical Sciences, Texas A&M University College of Dentistry, Dallas, Texas, USA

[f]Department of Organismal Biology and Anatomy, University of Chicago, Chicago, IL 60637 USA

Abstract

Mandible morphology has yet to yield definitive information on primate diet, probably because of poor understanding of mandibular loading and strain regimes, and overreliance on simple beam models of mandibular mechanics. We used a finite element model of a macaque mandible to test hypotheses about mandibular loading and strain regimes, and relate variation in muscle activity during chewing on different foods to variation in strain regimes. The balancing-side corpus is loaded primarily by sagittal shear forces and sagittal bending moments. On the working side, sagittal bending moments, anteroposterior twisting moments, and lateral transverse bending moments all reach similar maxima below the bite point, sagittal shear is the dominant loading regime behind the bite point, and the corpus is twisted such that the mandibular base is inverted. In the symphyseal region, the predominant loading regimes are lateral transverse bending and negative twisting about a mediolateral axis. Compared with grape and dried fruit chewing, nut chewing is associated with larger sagittal and transverse bending moments acting on balancing- and working-side mandibles, larger sagittal shear on the working-side, and larger twisting moments about vertical and transverse axes in the symphyseal region. Nut chewing is also associated with: higher minimum principal strain magnitudes in the balancing-side posterior ramus; higher sagittal shear-strain magnitudes in the working-side buccal alveolar process and the

balancing-side oblique line, recessus mandibulae and endocondylar ridge; and higher transverse shear strains in the symphyseal region, the balancing-side medial prominence and the balancing-side endocondylar ridge. The largest food-related differences in maximum principal and transverse shear strain magnitudes are in the transverse tori, and the balancing-side medial prominence, extramolar sulcus, oblique line, and endocondylar ridge. Food effects on strain regime are most salient in areas not traditionally investigated, suggesting that studies seeking dietary effects on mandible morphology might be looking in the wrong places.

Keywords

Chewing; Feeding; Electromyography; Strain; Finite element modeling (FEM)

1. Introduction

> "Strain gauges suffer from the limitation that they cannot sample the total strain environment. This is probably an intractable problem. On the other hand, lack of knowledge of biological parameters (masticatory force vectors and mandibular material properties) currently constrains finite element work; this problem may not be insoluble, but it is unlikely to be resolved in the near future. The errors in finite element models are not known, and a first step toward their assessment could be achieved by validating models with experimental strain data".
>
> (Daegling and Hylander, 2000: 549)

Despite decades of research into the relationship between the morphology and function of the hominid cranium, fundamental aspects of fossil hominid diet (what they ate) and feeding behavior (how they ate) remain unresolved (Grine et al., 2010; Ledogar et al., 2016; Rak, 1983; Robinson, 1972; Scott et al., 2005; Smith et al., 2015b; Spears and Macho, 1998; Strait et al., 2009a, 2013; Ungar et al., 2008). This is probably due, in part, to the fact that the cranium performs a variety of functions, making it difficult to identify signals of feeding adaptations that are unaffected by selection for other functions, such as orienting, housing, and protecting eyes, ears, and brains (Hylander et al., 1991; Lieberman et al., 2000; Ross et al., 2011; Ross and Iriarte-Diaz, 2014). As mandibles perform a narrower range of functions than the cranium, their morphology might display stronger covariation with diet and feeding behavior.

Current models of anthropoid primate mandible mechanics are based in large part on in vivo studies in macaques by W.L. Hylander in which hypotheses about mandibular stress, strain, and deformation regimes (sensu Ross et al., 2011) were derived from in vivo bone strain data from small areas of the corpus and symphysis (Hylander, 1977, 1979a, 1979b, 1979c, 1981, 1984, 1985, 1986, 1988; Hylander et al., 1987). In these studies, the in vivo data were explained and interpreted using simple beam models and assumptions about the relative magnitudes and orientations of the forces acting on the mandible during feeding. Subsequent studies then deployed the model to motivate morphometric studies of inter- and intraspecific variation in primate mandible form (Daegling, 1989, 1993, 2007a, 2007b; Daegling and Grine, 1991, 2006; Daegling and Hotzman, 2003; Daegling and Hylander, 1998, 2000;

Daegling et al., 1992; Dechow and Hylander, 2000; Demes et al., 1984; Hylander, 1979b, 1979c, 1984, 1985, 1988; Ravosa, 1991, 1996a, 1996b, 1999, 2000; Ravosa and Hogue, 2004; Ravosa and Simons, 1994; Ravosa et al., 2000; Taylor, 2002, 2005, 2006a, 2006b; Taylor et al., 2008; Vogel et al., 2014; Wolff, 1984). This intensive comparative morphometric research has yet to uncover strong relationships between mandible form, feeding behavior and diet in living primates (Daegling, 2007b; Daegling et al., 2016; Daegling and Grine, 2006; Hylander, 1988; McGraw and Daegling, 2012, 2020; Ravosa et al., 2016; Ross and Iriarte-Diaz, 2019b; Taylor, 2002, 2006a).

Several reasons for lack of a clear-cut relationship between mandibular morphology, feeding behavior and diet have been suggested (Daegling and Hylander, 2000; Ross and Iriarte-Diaz, 2014, 2019a; Ross et al., 2012; Taylor et al., 2008). One possibility is that simple beam models do not capture the complexity of mandibular strain regimes accurately enough, and that more realistic models would suggest that different kinds of measurements are needed, maybe in different places. The limitations of simple beam models—prismatic structure and homogeneous material properties—are widely acknowledged (Chalk et al., 2011; Daegling, 1993; Daegling and Hylander, 1998; Daegling and Hylander, 2000). The best method for overcoming these limitations is finite element modeling (FEM) wherein geometry and material properties can be represented more precisely than in a simple beam and the sensitivity of the model to their errors and variation can be quantified (Daegling and Hylander, 2000; Gröning et al., 2012; Moazen et al., 2009; Panagiotopoulou et al., 2017; Porro et al., 2011, 2013; Rayfield, 2011; Smith et al., 2015a, 2015b; Strait et al., 2005, 2007, 2009, 2010; Wroe et al., 2007). Moreover, FEMs make it possible to estimate strain regimes throughout the mandible, not just in the small areas historically sampled by strain gages, and to estimate all of the components of the strain regime— shear and principal strains.

Our understanding of primate mandible design—form-function relationships—might also be improved by better understanding of variation in external forces associated with different feeding behaviors and the impact of those loading regimes on mandibular strain regimes. For example, increased consumption of “tougher and more fibrous foods” (Hylander, 1979c: 294, 1985: 328) requires “recruitment of relatively greater amounts of balancing-side muscle force” (Hylander, 1985: 328–329), and this is hypothesized to require increased symphyseal strength to counter increased symphyseal stresses (Hylander, 1979c, 1985; Ravosa, 1996a, 1996b, 2000). However, the exact nature of those stresses is not known. Increases in vertical components of balancing-side muscle force would increase frontal shear stresses, whereas increases in transverse components would increase transverse bending—‘wishboning’—stresses. However, all jaw muscles generate forces with both vertical and transverse components, and the relative magnitudes of the associated moments can vary with changes in muscle activation and relaxation through the gape cycle (Hylander and Johnson, 1989, 1993, 1994; Hylander et al., 1987, 2000, 2002, 2004, 2005, 2011). Consequently, the effects of this force modulation on mandibular strain regimes are difficult to estimate with much precision. FEMs are also currently the best solution to this problem. Mandibular loading regimes can be precisely modeled using estimates of muscle forces based on electromyographic (EMG) and muscle architecture data, enabling more accurate and precise estimates of relative muscle force (Panagiotopoulou et al., 2017; Weijs and Dantuma, 1975, 1981; Weijs and Van der Wielen-Drent, 1982). When these data are combined with accurate

measures of muscle attachment locations and orientations, it is possible to make precise—and hopefully accurate—estimates of moments and shearing forces, enabling testing of hypotheses about mandibular loading regimes.

These advantages of FEM led us to develop a finite element model of the mandible of an adult female rhesus monkey (*Macaca mulatta;* Panagiotopoulou et al., 2017). The geometry of the model was based on CT scans of the animal's mandible, bone material properties were measured from the specimen post mortem (Dechow et al., 2017; Panagiotopoulou et al., 2017), and external forces were estimated using a combination of in vivo EMG and muscle architecture data collected from the same individual. The model was validated against in vivo strain gauge data recorded when the animal was chewing on three different food types: nuts, dried fruits and grapes (Mehari Abraha et al., 2019; Panagiotopoulou et al., 2017).

Here we deploy this model to address three questions. First, we ask whether the loading regime of our FEM—the combination of external forces acting on the mandible—and the FEMs deformation regime—the overall pattern of deformation—match current ideas about anthropoid mandible mechanics during the power stroke of mastication (Demes et al., 1984; Hylander, 1979b, 1979c, 1984, 1985, 1988; Hylander et al., 1987; van Eijden, 2000; Wolff, 1984).

Second, we ask what mandibular strain regime is associated with these loading and deformation regimes. Previous research has focused on strain regimes in the areas where strains have been recorded in vivo, especially the lateral prominence of the corpus and the labial surface of the symphysis, and made assumptions about patterns of strain in other areas. Here, we provide a more comprehensive description of strain regimes throughout the macaque mandible, including principal, axial and shear strains. This description contextualizes our discussion of food-related variation in strain regimes, provides novel insights into mandible mechanics during chewing, and suggests new hypotheses about mandible form-function relationships. This description also lays the groundwork for FEM analyses of hominid primate mandibles currently in preparation.

Lastly, we ask how variation in loading regimes associated with mastication on foods of different material properties affects deformation and strain regimes in the mandible. Specifically, we ask which areas of the mandible are most affected by variation in loading regime associated with variation in food material properties, and which strain components vary the most. These results are important for researchers interested in hominid evolution because they provide insight into the ability of traditional measures of mandible form—corpus and symphyseal external dimensions—to identify differences in feeding behavior or diet in extinct primates, and because they suggest new aspects of morphology for comparative and evolutionary analysis.

Terminology of mandible morphology and coordinate systems used to describe mandible morphology and loading, deformation, and strain regimes is given in Figure 1. The ramus is the mandible posterior to M_3 and includes the coronoid and condylar processes; the corpus of the mandible extends from below M_3 to a frontal plane through the back of the midline

symphyseal region, roughly level with the P_3s; the symphyseal region lies between the P_3s on each side. Inner and outer surfaces of the ramus are referred to as medial and lateral, of the corpus as lingual and buccal, and of the symphyseal region as lingual and labial. B) In transverse planes (seen from superior and inferior views), the V-shaped basal arch of the mandibular corpora converges on the symphyseal region more sharply and more posteriorly than does the U-shaped arch of the alveolar processes (Virchow, 1916, 1920; Weidenreich, 1936). Superiorly this exposes a chevron shaped planum alveolare, which is broad in the symphyseal region—lingual to the incisors, canines and P_3s—and tapers posteriorly into the alveolar process of the M_2 on each side. Where the V-shaped outline of the basal mandibular arch diverges posteriorly to grade into the rami, the alveolar processes of the M3 and the retromolar trigon curve lingually to form an alveolar prominence (prominentia alveolaris; Weidenreich, 1936) protruding over the submandibular fossa. Anteriorly this alveolar prominence is connected to the superior transverse torus of the symphyseal region by a variably developed and variably named ridge of bone: in *Homo* this has been referred to as a "slight bony ridge" (Gaspard, 1978: Fig. 6l), as an "alveolar prominence" sensu lato (Rightmire and Deacon, 1991; Weidenreich, 1936: 47), or perhaps as "torus alveolaris" (Weidenreich, 1936: 99). We suggest that alveolar prominence should be reserved for the posterior extremity of the medial prominence, in part because using that term to refer to the entire ridge of bone running anteriorly from the alveolar prominence sensu stricto gives the erroneous impression that the ridge is structurally, functionally or developmentally part of the alveolar process. We instead employ the term medial prominence of the corpus, or simply medial prominence to refer to the ridge of bone connecting the superior transverse torus of the symphyseal region with the alveolar prominence at the back end of the tooth row. Together these three structures form the lingual outline of the upper mandibular corpus and symphysis, Virchow's arcus intermedius, and Weidenreich's inner mandibular arch (Virchow, 1920; Weidenreich, 1936).

The mylohyoid line is distinct from the medial prominence, although the line crosses the prominence in its course from the ramus to the symphyseal region. When it is well defined the mylohoid line extends from the inferior transverse torus to the ramus below (and, sometimes in humans, at) the torus triangularis. As it crosses the alveolar prominence the mylohyoid line angles anteroinferiorly, leaving room for the lingual nerve to enter the floor of the mouth between the medial edge of the posterior alveolus and the mylohyoid muscle. The internal oblique line of dental radiology corresponds to the mylohyoid line (and sometimes torus triangularis). A variably robust ridge of bone extending posteriorly from the alveolar prominence to the condylar neck is divided into, from front to back, the crista pharyngea, torus triangularis, and endocondylar crest (Gaspard, 1978; Piveteau, 1957; Weidenreich, 1936) or endocondylar ridge (White et al., 2012). An endocoronoid crest diverges from torus triangularis and extends superiorly towards the tip of the coronoid process. Anterior to the endocoronoid crest the front edge of the ramus is marked by the temporal crest, which splits to enclose a shallow recessus mandibulae (Lenhossek, 1920), which in turn opens inferiorly into the extramolar sulcus (Keiter, 1935). Lateral to this sulcus the anterior edge of the ramus continues down onto the buccal corpus as the external oblique line of the mandible, which merges with the lateral prominence (Rasche, 1913) below M_3.

Definitions of terms used to describe loading, deformation and strain regimes follow Ross et al. (2011). Loading regime refers to the combination of external forces acting on the mandible, in vivo or in silico. Loading regimes are summarized here as shear forces and twisting moments or torques. Stress and strain regimes are the patterns of internal forces and strains within the mandible or FEM associated with a given loading regime. Here the strain regimes are the axial, principal and shear strains in the surface of the model. Deformation regimes are the patterns of deformation of the mandible—the integral of the strain regime across the mandible—associated with the loading regimes. Here the deformation regimes are bending, shearing and twisting within and about specified axes and planes.

To facilitate comparisons with prior literature, loading, strain, and deformation regimes are described in an anatomical coordinate system aligned with a right-handed Cartesian coordinate system. The X-axis is superoinferior (SI); the Y-axis is anteroposterior (AP); the Z-axis is mediolateral (ML). In this paper, the term ‘mediolateral axis’ is preferred over ‘transverse axis’ to minimize confusion with references to the transverse plane. XY planes are sagittal planes, XZ planes are frontal (coronal) planes, and YZ planes are transverse planes. Shear forces act within named planes: sagittal shear forces act within sagittal planes, frontal shear forces within frontal (coronal) planes, and transverse shear forces within transverse planes. Following Hibbeler (2000), positive shear forces rotate bodies clockwise looking from the right side, top, or front (i.e., towards the origin of the coordinate system). Shear forces are associated with sagittal, frontal and transverse shear strains and deformations in those planes. Positive shear strain is a decrease in the angle of the corner of a square element at the intersection of the coordinate system axes. Moments or torques are described as acting about anatomical axes, with positive and negative moments following the right-hand rule. Moments around the Y or AP axis that tend to evert the base of the right mandible or invert the base of the left mandible are negative AP moments or torques. Positive moments around a vertical (X) axis through the right mandible—laterally wishboning the balancing-side mandible—are positive SI moments or torques. Positive moments about an ML axis are positive ML moments or torques. Because of the shape of the mandible: AP moments (torques about AP axes) through the corpus and ramus are twisting moments; ML moments (torques about ML axes) through the corpus and ramus are sagittal bending moments; ML moments through the symphyseal region are ML twisting moments; and SI moments anywhere through the mandible are transverse bending moments. Positive sagittal bending is concave superiorly (the shape holds water; Hibbeler, 2000). Axial strains are positive (tensile) or negative (compressive) strains in planes parallel to the coordinate system axes. Although axial strains are not usually discussed in the literature, they provide useful insight into the strain and deformation regimes associated with calculated loading regimes.

A variety of theories of mandible mechanics have been proposed. In this paper we focus on those that have been most influential on ideas about anthropoid primate mandible mechanics and on the kinds of bony measurements that functional morphologists use to study links between mandibular form and feeding behaver or diet.

The balancing-side corpus

According to current theories of mandible mechanics the balancing-side corpus is subject to negative sagittal bending (concave inferiorly), negative sagittal shear (more posterior sections are forced superiorly relative to more anterior sections), lateral transverse bending (lateral 'wishboning'), and negative AP twisting (eversion of the basal border; Hylander, 1979b, 1979c, 1981, 1985). For definitions of the coordinate system and terms such as negative bending and negative shear, see Figure 1. Sagittal shear forces are hypothesized to be greatest in the ramus, between points of application of muscle and joint forces (van Eijden, 2000), or in the corpus (Demes et al., 1984); lateral transverse bending moments are hypothesized to increase from posterior to anterior (van Eijden, 2000), and AP twisting moments are expected to be constant along the corpus (Demes et al., 1984; Hylander, 1979c). A human-like deformation pattern would be "helically upward and towards the working-side" (van Eijden, 2000: 131), with sagittal deformation and negative twisting—eversion of the basal border (Korioth et al., 1992).

The working-side corpus

The working-side corpus below the postcanine teeth is hypothesized to be subject to positive sagittal bending, positive sagittal shear, lateral transverse bending, and AP twisting that varies with bite point (Hylander, 1979b, 1979c, 1981, 1985). In chewing or biting along the anterior postcanine teeth, as modeled here, the anterior corpus is subject to negative AP twisting (inversion of the basal border) and the ramus is subject to positive AP twisting (eversion of the basal border). Sagittal shear is hypothesized to be largest between the bite point and the muscle insertion points on the ramus (Demes et al., 1984; Hylander, 1979c; van Eijden, 2000); lateral transverse bending moments are hypothesized to increase from posterior to anterior (van Eijden, 2000; Vinyard and Ravosa, 1998) or to peak at the bite point (Demes et al., 1984); and AP twisting moments are argued to vary with bite point, with relative magnitudes of muscle and bite force, and along the corpus (Demes et al., 1984; Hylander, 1979c). Human-like deformation of the working-side mandible has been described as a predominance of sagittal bending over twisting, with the twisting characterized by inversion of the basal border (Korioth et al., 1992).

The symphyseal region

The symphyseal region is hypothesized to be subject to positive frontal bending, negative frontal shear, lateral transverse bending, and negative ML twisting (Hylander, 1984). Positive frontal bending is thought to be the result of a combination of negative AP torsion of the balancing-side mandible and positive AP torsion of the working-side—eversion of the basal mandible on both sides. Negative frontal shear is thought to be due to a combination of superior components of balancing-side muscle force and inferior components of bite force (Beecher, 1977; Demes et al., 1984; Hylander, 1984; Korioth and Hannam, 1994; Korioth et al.,1992). Lateral transverse bending late in the power stroke is hypothesized to be due to laterally (to the balancing-side, to the right in our model) directed components of balancing-side deep masseter force pulling the balancing-side mandible laterally, while the bite force and residual (decreasing) force from the working-side superficial masseter pull the working-side mandible in the opposite direction (Hylander, 1984; Hylander and Crompton, 1986;

Hylander and Johnson, 1994, 1997; Hylander et al., 1987). The question of the direction of ML twisting is as yet unresolved: some authors posit that positive twisting occurs because the moments associated with upward components of balancing-side muscle force are larger than moments associated with inferiorly directed joint-reaction force (Wolff, 1984; Wolpoff, 1980). Others hypothesize negative ML twisting due to large torques associated with the balancing-side joint-reaction force (Hylander, 1984).

The ramus

The inaccessibility of the ramus for in vivo strain gage recordings has resulted in its neglect in most recent work on primate mandible biomechanics. Older studies suggested that various external features of the ramus, including the endocondylar ridge, ectocondylar crest, endocoronoid crest, and external oblique line function to strengthen the ramus against muscle forces being transmitted to the corpus (Walkhoff, 1902; Weidenreich, 1936). As noted above, in chewing or biting along the anterior postcanine teeth the ramus is hypothesized to be subject to positive AP twisting and sagittal shear is hypothesized to be largest between the bite point and the muscle insertion points on the ramus (Demes et al., 1984; Hylander, 1979c; van Eijden, 2000).

2. Materials and methods

The finite element model used in this paper is that presented by Panagiotopoulou et al. (2017). We used the material properties, loading, and constraint conditions that resulted in the best validated model from that study. The geometry of the skull was captured with computed tomography (CT) on a Philips Brilliance Big Bore scanner at the University of Chicago. Scans were processed in Mimics Materialise software v. 17 (Materialise, Belgium) to segment out the mandible and extract 3D surface datasets of the cortical bone, trabecular bone tissue, teeth, periodontal ligament (PDL), and mandibular bone screws (used to measure jaw kinematics). The bone screws (2.7 mm × 10 mm Vitallium cortical bone screws [OFSQ13; 3I Implant Company, West Palm Beach, FL, USA]) were included in the model because they were present in the animal during the in vivo validation recordings reported in Panagiotopoulou et al. (2017). The 3D data sets of all materials were assembled to create a 3D non-manifold file in Materialise 3-matic v. 10 (Materialise, Belgium) and converted into volumetric mesh files of solid continuum linear tetrahedral elements (C3D4) for finite element analysis (FEA). The whole assembly has 622,134 elements and the maximum nominal element size is 0.7 mm.

Isotropic, homogeneous and linear elastic material properties were assigned to the PDL ($E = 6.80 \times 10^{-4}$ GPa; $v = 0.49$), teeth ($E = 24.5$ GPa; $v = 0.3$), bone screws ($E = 105$ GPa; $v = 0.36$), and trabecular bone tissue ($E = 10$ GPa; $v = 0.3$; Panagiotopoulou et al., 2017). The cortical bone was modeled as heterogeneous and orthotropic using subject-specific measurements of bone properties with the ultrasound wave technique (Dechow et al., 2017). Tie constraints (frictionless constraints) were used to bind together all intersecting surfaces.

To simulate the bite force we constrained all translations at nodes on the occlusal surface of the left P_3 (35 nodes), P_4 (32 nodes), and M_1 (78 nodes). One node on the top of the left (working-side) mandibular condyle was fixed against displacement in all directions; one

node at the top of the right condyle was fixed against AP and SI but not ML displacement (Panagiotopoulou et al., 2017).

To determine how mastication on foods of different material properties affects deformation and strain regimes in the mandible we applied three different loading regimes, associated with chewing on foods of three different material property types—fresh grapes with skins, dried fruits, and nuts (Reed and Ross, 2010). Muscle force magnitudes were estimated using in vivo EMG data recorded during a single feeding session in which the animal fed on softer food (grapes) with relatively low toughness ($R = 125\ Jm^{-2}$) and low stiffness ($E = 0.6$ MPa), dried fruits (prune, dry apricot/cranberry/pineapple, date, gummy bear) characterized by relatively high toughness ($590 \leq R \leq 1059\ Jm^{-2}$) and low stiffness ($0.5 \leq E \leq 6.0$ MPa), and nuts (shell-less almond, cashew, brazil nut, pecan, walnut), characterized by relatively low toughness ($105 \leq R \leq 166\ Jm^{-2}$) and high stiffness ($8 \leq E \leq 34$ MPa; Reed and Ross, 2010; Ross et al., 2009; Williams et al., 2005; Supplementary Online Material [SOM] Fig. S1). The highest EMG amplitude recorded from each muscle was assumed to correspond to recruitment of 100% of that muscle's physiological cross-sectional area (PCSA) and the EMG amplitudes were scaled linearly (Weijs, 1980; Weijs and Dantuma, 1975; Weijs and Van Ruijven, 1990).

Estimates of muscle PCSAs for our experimental subject were made following standard dissection methods described elsewhere (Anapol et al., 2008; Shahnoor, 2004; Taylor et al., 2009, 2015; Taylor and Vinyard, 2009, 2013) using the following equation:

$$\text{PCSA } (cm^2) = (\text{muscle mass [g]} \times \cos\theta)/(\text{fiber length [cm]} \times 1.0564\ g/cm^3),$$

where $1.0564\ g/cm^3$ is the specific density of muscle (Mendez and Keys, 1960), normalizing fiber length by sarcomere length following Felder et al. (2005). Instantaneous force estimates were calculated as the mean normalized EMG amplitude at time of maximum strain magnitude in the lower lateral gage × estimated PCSA × specific tension of muscle ($30\ N/cm^2$; Sinclair and Alexander, 1987). Muscle forces were applied at surface nodes representing the insertion of the jaw muscles—anterior and posterior temporalis, deep and superficial masseters, and medial pterygoids—estimated from dissection of the experimental subject (SOM Fig. S1). Muscle force orientations were calculated using vectors running from the centroids of the insertions on the mandible to the centroids of the origins on the cranium (SOM Fig. S2; Panagiotopoulou et al., 2017). Table 1 gives the X, Y, Z components of the muscle force vectors estimated from EMGs recorded during chewing of the three food types, as well as the components of the reaction-force vectors acting at the condyles and bite points.

Loading regimes were quantified using moments and shear forces. Following convention, twisting moments (torques) act about the long (AP, Y) axis of the mandible and bending moments act about the orthogonal axes. Sagittal bending moments act about the transverse (ML, Z) axis, and transverse bending moments act about the vertical (SI, X) axis. Moments were calculated in Abaqus CAE Simulia v 6.13 (Dassault Systemes, Velizy-Villacoublay, France) about coordinate axes through centroids of cross-sections (Fig. 2). Shear forces pull adjacent parts of the mandible in opposite directions and are calculated in sagittal (XY),

frontal (XZ) and transverse (YZ) planes (Fig. 3). Shear forces were calculated in Excel 2010 (Microsoft Corporation (Redmond, Washington, USA).

FEMs were solved using the Abaqus default implicit direct static solver and Newtonian default iterations. Solution time, using four processors and eight tokens, was approximately ten minutes per model. Deformation regimes were examined using static images of deformed and undeformed models (SOM Fig. S3) as well as animations of 1–70× scaled deformations of the deformed model (SOM File S1). It is important to note that the animations in SOM Figure S1 are not dynamic representations of changing patterns of deformation through the power stroke: rather, they show linear increases in deformation magnified 70×. The distributions of axial (X, Y, Z), principal and shear strains were examined using figures of the models with colors representing strain magnitudes. In order to compare strain regimes associated with different food types, strain magnitudes were extracted from surface elements under different loading conditions, then the difference values were calculated and plotted on the surface of the models using a color scale.

All in vivo primate work was done at the University of Chicago under Animal Care and Use Protocol 72154

3. Results

3.1. Loading, deformation and strain regimes during chewing

We first asked whether loading and deformation regimes in our macaque FEM match those hypothesized for the power stroke of mastication (Dechow and Hylander, 2000; Demes et al., 1984; Hylander, 1979b, 1979c, 1984, 1985, 1988; Hylander et al., 1987; Korioth et al., 1992; van Eijden, 2000; Wolff, 1984). Hypotheses about loading and deformation regimes underlie decisions about measurements made by functional morphologists attempting to link mandibular morphology to feeding behaviour and diet. This question was addressed using results from modeling of nut chewing during which moments, shear forces, and strain magnitudes were the highest in comparison with other food types. We then described the strain regimes in the corpus, ramus and symphysis associated with these loading and deformation regimes. Loading regimes are given in Figure 3. Deformation and strain regimes for the balancing side are shown in Figure 4, for the working side in Figure 5, and for the symphyseal region in Figure 6. Axial, shear and principal strains during nut chewing are shown in SOM Figures S4–S7. Deformation animations are shown in SOM File S1.

3.2. Balancing-side (right) corpus

Loading and deformation regime—Consistent with our hypothesis, the balancing-side corpus is subject to negative sagittal bending, negative sagittal shear, lateral transverse bending and negative AP twisting. The largest torques acting on the balancing-side mandible are positive ML—negative sagittal bending—moments associated with inferiorly directed components of bite force transmitted across the symphysis (Fig. 2). These moments increase posteriorly until opposed by the negative torques exerted by superior components of balancing-side jaw-elevator muscles (Fig. 2, frontal section No. 13). Negative sagittal bending moments are accompanied by negative sagittal shear forces (Fig. 3C), which are due

to inferiorly directed components of force crossing the symphysis from the biting side, superiorly directed components of balancing-side jaw elevator muscles acting on the ramus, and inferiorly directed components of joint-reaction force (Fig. 4B, F). These negative sagittal shear forces, larger in the posterior ramus than the corpus (e.g., van Eijden, 2000), deform the balancing-side angle, ramus and coronoid process upwards relative to the corpus (Fig. 4A, B).

The balancing-side mandible is also subjected to negative vertical torques (Fig. 2)—and associated positive transverse shearing forces (Fig. 3D)—which produce lateral transverse bending deformation of the balancing-side (right) angle, condyle, ramus, and most of the corpus (Fig. 4A, B; SOM Figs. S5 and S6). The balancing-side mandible is also subject to low magnitude negative AP torques (Fig. 2), causing eversion of the basal border (Hylander, 1979c; Fig. 4A; SOM Fig. S6). However, rather than being constant along the corpus (Demes et al., 1984; Hylander, 1979c), these AP torques increase in the anterior corpus, peaking at the level of P_4.

The overall deformation of our macaque FEM (SOM Fig. S6) resembles that of the model of a human mandible by Korioth et al. (1992: Fig. 3; see also Korioth and Hannam, 1994): in deformation, the mandible appears to rotate around the bite point, with the balancing-side mandible basal border everting and the alveolar process inverting.

Strain regime—Negative sagittal bending of the balancing-side corpus is associated with high magnitude tensile AP and ε_1 strains on the superior and medial surfaces of planum alveolare, the extramolar sulcus, and the alveolar prominence (Fig. 4H, I). Sagittal shear forces are associated with negative sagittal shear strain in the buccal surface of the corpus, especially the external oblique line (Fig. 4F, G). Lateral transverse bending is associated with tensile AP strain and high magnitude ε_1 on most of the lingual surface (Fig. 4I), compressive AP strain on the buccal surface of the mandible (Fig. 4J), and positive transverse shear strains on the superior surface of planum alveolare, the extramolar sulcus, and the alveolar prominence (SOM Fig. S5N, Q). AP compression is not uniformly distributed on the buccal surface; superposition of lateral transverse bending on negative sagittal bending results in high values of AP compression (Fig. 4K) and ε_2 on the buccal aspect of the basal corpus (Fig. 4L). Negative AP torsion of the balancing-side mandible is associated with positive transverse shear strain on the superior surface of the planum alveolare, the extramolar sulcus, and the alveolar prominence (Fig. 4C) combined with negative transverse shear strains on the basal surface (Fig. 4D).

3.3. Working-side (left) corpus

Loading and deformation regime—As hypothesized, the working-side mandible below the bite point on P_4 and M_1 is subjected to negative ML (positive sagittal bending) moments, positive vertical (lateral transverse bending) moments, and negative AP moments. The effects of these torques on the anterior working-side corpus—under the bite point—are positive sagittal bending, lateral transverse bending, and negative AP torsion, inverting the basal border below the bite point (Fig. 5A, B; SOM Fig. S6). Torques are not constant along the corpus: in the posterior corpus, transverse, vertical, and AP torques decrease to zero at or

immediately behind M_3 before reversing in the ramus (see below; Fig. 2). Despite this reversal, the basal border of the entire working-side mandible is inverted in deformation (SOM Fig. S6). As hypothesized, sagittal shear forces are highest between the bite points on the tooth row and the ramus (Demes et al., 1984; Hylander, 1979c; van Eijden, 2000). However, contrary to our hypothesis, negative (as opposed to positive) sagittal shear is high along the length of the mandible (Figs. 3, 5F), deforming the retromolar fossa upwards (Fig. 5B; SOM Fig. S6).

Strain regime—Positive sagittal bending deformation about the bite point is associated with compressive AP strain along the buccal and lingual sides of the alveolar process and in the upper surface of planum alveolare lingual to the premolars, canines and incisors (Fig. 5H, J, K). It is also associated with relatively high magnitude tensile AP and ε_1 strains in the base of the corpus below the bite point (Fig. 5K–M). On the buccal surface of the working-side corpus, AP variation in shear forces is associated with variation in sagittal shear strains: these shear strains are positive in front of the bite point, negative immediately behind it and then positive further posteriorly, in the ramus (Fig. 5F, G). Negative AP torsion of the anterior working-side corpus is associated with positive transverse shear strain on the superior surface of the corpus and negative transverse shear strain in the base of the mandible (Fig. 5C, D). ε_1 is oriented upwards and backwards on the buccal side of the corpus, below m_3, and upwards and forwards on the lingual side (Panagiotopoulou et al., 2017: Fig. 10).

3.4. Symphyseal region

Loading and deformation regime—A hypothesis of positive frontal bending is corroborated by the moments acting on the symphysis (Fig. 2) and by the deformation regime (Fig. 6A, E; SOM Fig. S6). However, contrary to accepted models (Beecher, 1977; Hylander, 1984), this positive frontal bending is associated with negative AP moments in both working- and balancing-side mandibles (Fig. 2; SOM Fig. S6). These moments, maximum in a near-frontal plane through the balancing-side P_4 and working side M_1, twist the symphysis and balancing-side corpus about the bite point, resulting in positive frontal bending deformation, with a center of flexure at the bite point (clockwise in anterior view; Figs. 4C, D and 5C, D; SOM Fig. S6). A hypothesis of negative frontal shear deformation of the symphysis is corroborated by the loading (Fig. 3) and deformation regimes (Fig. 6E; SOM Fig. S6). However, if negative frontal shear loading and deformation regimes were predominant in the symphyseal region, both labial and lingual surfaces of the symphysis would experience negative frontal shear strain. In contrast, negative frontal shear strain in the labial surface (Fig. 6H) is accompanied by positive frontal shear strain in the lingual surface (Fig. 6D; see below). Similarly, the symphyseal region is also characterized by transverse shear of opposite signs on superior and inferior surfaces (Fig. 7J; SOM Fig. S5Q, R). Shear strains of opposite sign on opposing surfaces are indicative of torsion and the loading and deformation regimes confirm a hypothesis of negative ML twisting (Hylander, 1984), not positive ML twisting (Demes et al., 1984; Wolff, 1984; Wolpoff, 1980; Fig. 6I–K). These negative ML twisting moments are primarily because of large inferiorly directed components of balancing-side joint-reaction force (−100 N) acting about a long moment arm (0.064 m), yielding a negative ML torque of 6.4 Nm (Fig. 6I). This is countered by positive

ML torques associated with anteriorly directed components of balancing-side joint reaction force and superior components of balancing-side jaw elevator muscle force, but the net effect is a negative 0.7 Nm ML twisting moment through the symphysis (Fig. 6I–K). The deformation regime of the symphyseal region provides visual confirmation of the loading regime: the anterior region of the balancing-side mandible deforms upwards relative to the jaw joint (Fig. 6E; SOM Fig. S6).

A hypothesis of lateral transverse bending (lateral 'wishboning') is corroborated by the negative vertical torques in the balancing-side symphyseal region (Fig. 2), negative transverse shear forces on the working-side symphysis, and positive transverse shear forces on the balancing- side symphysis (Fig. 3). As a result, the balancing-side condyle, angle, and corpus are deformed laterally relative to the working-side (Fig. 6A, E).

Strain regime—Lateral transverse bending of the symphyseal region is associated with high values of ML directed tensile strain in the lingual symphysis (Fig. 6B, C), and ML oriented compressive strain in the labial symphysis (Fig. 6F, G; Hylander, 1984). As discussed above, negative ML twisting of the symphysis is associated with negative frontal shear strain on the labial surface and positive frontal shear strain on the lingual surface (Fig. 6D, H, K), along with positive ML shear strain on the superior surface and negative ML shear strain on the inferior surface (SOM Fig. S5Q, R).

The strain regime does not support the hypothesis that the symphysis is bent in frontal planes due to positive AP twisting of the working-side mandible and negative AP twisting of the balancing-side (Demes et al., 1984; Wolff, 1984). This loading regime would result in ML tensile strain in the lower half of the labial and lingual symphysis and ML compressive strain in the upper half of the symphysis. In fact, the entire midline lingual symphysis is in ML tension and the lower labial symphysis is in ML compression.

3.5. The ramus

Loading and deformation regime—The balancing-side ramus experiences large positive ML—negative sagittal bending—moments, which peak in frontal sections through the anterior ramus, external oblique line, and mandibular prominence, combined with low magnitude negative AP moments and large positive sagittal shear forces (Figs. 2 and 3; SOM Fig. S6). The working-side ramus is subject to positive ML—negative sagittal bending—moments, the reverse of the negative bending regime acting around the bite point. The working-side ramus is also subject to small positive AP twisting moments, as well as positive transverse and sagittal shear forces (Figs. 2 and 3).

Strain regime—Negative sagittal bending of the balancing-side ramus is associated with high magnitude tensile AP and ε_1 strains on the superior surfaces of the extramolar sulcus, the anterior border of the ramus, the external oblique line, torus triangularis, and the endocondylar ridge (Fig. 4E, H, I). High magnitude compressive AP and ε_2 strains are seen in the basal border of the ramus (Fig. 4J–L). Increasingly positive sagittal shear forces in more posterior sections are associated with a transition from high negative sagittal shear strains in the external oblique line to positive sagittal shear strains in the angle and posterior condylar neck (Fig. 4F, G). Lateral transverse bending and negative AP torsion of the

balancing-side ramus result in positive transverse shear strains in the endocondylar ridge and the mandibular notch (Fig. 4C). The medial surface of the working-side ramus experiences mostly low strain magnitudes, with the exception of positive sagittal shear strains along the endocondylar ridge and the back edge of the ramus (Fig. 5G; SOM Fig. S5B).

On the working-side, negative sagittal bending is also associated with high magnitude tensile AP and ε_1 strains on the superior surfaces of the extramolar sulcus, the anterior border of the ramus, torus triangularis, and the endocondylar ridge (Fig. 5E, I, J), combined with high magnitude compressive AP and ε_2 strains on the basal border (Fig. 5J, L, N). Sagittal shear strains in the lateral surface transition from high negative strains in the oblique line to positive strains in the angle and posterior condylar neck (Fig. 4F, G). Positive AP—twisting—moments in the working-side ramus are associated with negative transverse shear strains in the extramolar sulcus, torus triangularis, endocondylar ridge and mandibular notch (Fig. 5C), and with positive transverse shear strains on the basal border and angle (Fig. 5D).

In both working-and balancing-side rami, SI tensile strains are high along the anterior edge of the ramus and SI compressive strains are high along the posterior edge of the ramus (SOM Fig. S4A, B).

3.6. Effects of variation in food type: Balancing-side (right) mandible.

Loading and deformation regime—Hypothesized effects of food material properties on mandibular loading and deformation regimes underlie attempts to link mandibular morphology to diet and feeding behavior. Loading regimes—moments and shear forces—associated with chewing on grapes, dried fruits and nuts are shown in Figures 2 and 3; differences in loading regime between nut and dried fruit chewing, and between nut and grape chewing, are shown in Figures 7 and 8. On the balancing-side, loading regimes during nut chewing are similar to those during dried fruit and grape chewing (Figs. 2 and 3), but nut chewing is associated with larger positive ML (sagittal bending) and larger negative vertical (lateral transverse bending) moments under the postcanine tooth row (Fig. 7), and larger vertical and transverse shear forces (Fig. 8). The largest differences in AP twisting moments are found under P_3; these are the smallest food-related effects on the balancing-side.

Strain regime—Figure 9 compares the magnitudes of the principal and shear strains across the surface of the model, calculated as ([nut strains] – [fruit strains]). As expected with higher sagittal bending moments, principal and shear strain magnitudes are higher during simulated nut chewing than dried fruit chewing. The greatest differences in ε_1 between nuts and dried fruit are seen in the lingual symphysis (see below) and balancing-side mandible. ε_1 magnitudes are higher during nut chewing than dried fruit chewing in (i) the inferior transverse torus, (ii) an oblique line extending from the superior transverse torus along the balancing-side medial prominence towards the M_3 (Fig. 9A, C), (iii) the balancing retromolar trigon and extramolar sulcus (Fig. 9B), and (iv) the endocondylar ridge (Fig. 9C). Differences in ε_2 strain magnitude are concentrated in the alveolar bone around the roots of the biting teeth (Fig. 9E–H) and in the posterior edge of the balancing-side ramus, below the condyle (Fig. 9G).

There are large differences in magnitudes of balancing-side shear strains between nut and dried fruit chewing (Fig. 9I–T). The largest differences are in sagittal shear strains: during nut chewing sagittal shear strains are larger in the front of the condylar neck, on the upper surface of the endocondylar ridge, on the lingual face of the balancing-side coronoid process, in the extramolar sulcus, and across most of the buccal side of the balancing-side corpus and symphysis (Fig. 9I–L). During nut chewing the balancing-side mandible also experiences larger positive transverse (ε_{yz}) shear strains in the superior transverse torus of the symphyseal region, the medial and alveolar prominences, retromolar trigon, extramolar sulcus, torus triangularis, and endocondylar ridge (Fig. 9Q). These differences are associated with, and reflect, greater bending and torsion of the balancing-side mandible, and larger vertical and transverse shear forces during nut chewing.

3.7. Effects of variation in food type: Working-side (left) mandible

Loading and deformation regime—On the working-side, compared with grape and dried fruit chewing, nut chewing is associated with (Figs. 7 and 8): larger positive ML (negative sagittal bending) moments acting on the working-side ramus; larger negative ML (positive sagittal bending) moments immediately behind the bite point; larger positive vertical (transverse bending) moments on the symphysis; larger negative AP twisting moments around the bite point; and larger negative transverse shear forces, especially in the anterior corpus.

Strain regime—Differences in strain regime between nut and dried fruit chewing are less pronounced on the working-side than the balancing-side. Higher magnitudes of ε_2 (Fig. 9E–H) and sagittal shear strain are evident in the lateral alveolar process around the working-side postcanine tooth roots (Fig. 9I–L). In association with increased sagittal shear forces, nut chewing is also associated with higher magnitude negative sagittal shear strains in the buccal surface of the working-side corpus below the molars, the working-side lateral prominence, and the external oblique line (Fig. 9I–L). The other principal and shear strain components in the working-side mandible are minimally impacted by variation in food type (Fig. 9).

3.8. Effects of variation in food type: Symphyseal region

Loading regime—Moments about frontal planes through the symphyseal region differ with food type (Figs. 2 and 7). During soft food (grapes) and nut chewing, the posterior symphyseal region is subjected to greater vertical moments (wishboning), and greater torques than during dried fruit chewing. However, the magnitudes of torques acting in frontal planes through the symphysis are low. The largest differences are in moments calculated about sagittal sections. Relative to the other foods, nut chewing is associated with larger negative vertical moments, especially in the midline, and larger AP twisting moments and ML (sagittal bending) moments.

Strain regime—There are large differences between nut and dried fruit chewing in strain magnitudes in the lingual symphysis. In both transverse tori, greater lateral transverse bending moments during nut chewing are associated with relatively higher magnitudes of ε_1 (Fig. 9C), and larger ML moments are associated with slight increases in negative sagittal

(Fig. 9K) and positive frontal shear strains (Fig. 9O). In the inferior transverse torus, negative transverse shear strain is also greater during nut chewing (Fig. 9S). On the labial surface of the symphysis ε_2 is larger inferiorly during nut chewing (Fig. 9H) and all of the shear strain components increase in magnitude. Sagittal shear strains become more negative on the balancing-side, and more positive on the working-side of the labial surface (Fig. 9L); coronal shear strains become more negative, especially on the inferior half of the balancing-side (Fig. 9P), and transverse shear strains becomes more negative on the balancing-side (Fig. 9T). These increases in shear strains reflect increased—more negative—ML torques associated with nut chewing.

3.9. Maximum food type differences

The largest food-related differences in strain magnitude are mapped onto the mandible in Figure 10. Notable differences in magnitudes of principal strains and in sagittal and frontal shear strains are restricted to localized areas. For example, large differences in ε_2 magnitude are restricted to the posterior condylar neck and ramus on the balancing-side (Fig. 10G). Large differences in sagittal shear strain magnitudes are restricted to the buccal alveolar process on the working-side and to recessus mandibulae and the lingual condylar neck on the balancing-side (Fig. 10I). Large differences in frontal shear-strain magnitudes are found in the inferior transverse torus (Fig. 10O, P). More significant are the large differences in ε_1 and transverse shear strains on the balancing-side, extending from both the superior and inferior transverse tori along the anterior medial prominence, through the extramolar sulcus, and along the endocondylar ridge (Fig. 10A–D, Q–T). Maximum differences in the orientation of the maximum principal strains are shown in Figure 11. Food type effects on strain orientation are concentrated in the area of the working-side bone screw callus, the anterior condylar neck, and in a strip along the lingual surface of the working-side corpus below the mylohyoid line.

4. Discussion

This is the most detailed analysis of in vivo loading, deformation, and strain regimes in a mammalian mandible published to date, but some limitations should be borne in mind. Our focus is on hypotheses specific to *Macaca* because macaque in vivo strain data have provided the model for so much of the comparative work on mandibular form and diet in primates. However, similarities in mandible shape (Daegling, 2002) and muscle firing patterns across anthropoids (Hylander, 1981, 1984, 1988; Hylander and Crompton, 1986; Hylander and Johnson, 1994, 1997; Hylander et al., 1987, 1998, 2000, 2002, 2004, 2005, 2011) make our results relevant especially to cercopithecids, but also to other anthropoids, including humans and other hominids. The present study also only documents loading, deformation, and strain regimes at one point in time during the gape cycle: when, during our in vivo recordings, peak shear strain magnitudes were recorded from the lower half of the lateral prominence on the corpus. Mandibular loading and strain regimes vary throughout the gape cycle (Hylander et al., 1987; Ross and Iriarte-Diaz, 2019a). Thus, ongoing studies are aimed at a fuller understanding of mandible biomechanics throughout the power stroke. It should also be noted that the modeled mandible exhibited bone calluses superior to the two lateral bone screws, and these may have affected the local strain environment. Consequently,

our discussion of strain regimes emphasizes strains in other parts of the mandible. Finally, we also note that transverse bite forces at the P_3 act towards the right, the reverse of the direction at the P_4 and M_1. This occurs because fixing the tooth surface against displacement fixes it against forces either pushing or pulling against the tooth surface. This effectively reduces the laterally directed component of bite force and negative torques acting on the anterior working-side tooth row. Our emphasis on modeling the in vivo experimental context as accurately as possible caused us to retain the excess bone and the fixed P_3 in this version of our model, the latter because these constraining conditions yielded the strain values that most closely matched those previously recorded in vivo (Panagiotopoulou et al., 2017).

4.1. Loading regimes

Current theories of macaque mandibular function make assumptions about the loading regime (Hylander, 1979b, 1979c, 1981, 1984, 1986; Hylander et al., 1987) and these assumptions underlie hypotheses about mandible design in extant and fossil hominids (Daegling, 1989, 2001, 2007a, 2007b; Daegling et al., 2016; Daegling and Grine, 2006; Hylander, 1988; Ravosa, 1988, 2000; Taylor, 2002, 2006a, 2006b). Most of these assumptions have not been tested because the necessary combination of EMG, PCSA, anatomical and strain data has not been available until recently (Panagiotopoulou et al., 2017). In the present study, mandibular loading regimes were calculated using EMG data collected when in vivo strain magnitudes in the lower lateral prominence of the working-side mandible were at their peak. At this time EMG activity has peaked in the working and balancing superficial masseters, anterior temporales and medial pterygoids, as well as in the working-side posterior temporalis, and is decreasing in amplitude. In contrast, EMG amplitudes in the balancing-side deep masseter and posterior temporalis are at their peak (SOM Fig. S1).

Hylander et al. (1987) reported that late activity in the balancing-side deep masseter was accompanied by decreased activity in the balancing-side medial pterygoid and increasing activity in the working-side medial pterygoid. They hypothesized that this combination of muscle forces resulted in large lateral transverse bending moments on the mandible, producing wishboning of the symphyseal region late in the power stroke (Hylander, 1984; Hylander et al., 1987). In contrast, our EMG data show that both medial pterygoids display decreasing EMG activity at the time when the balancing-side deep masseter is showing peak activity. Consequently, when our data are used to calculate the moments acting on the mandible, the loading regime on the balancing-side corpus is dominated by sagittal shear forces and sagittal bending moments (Figs. 3C and 4F, G); lateral transverse bending moments are comparatively low. The balancing-side corpus does experience negative AP—twisting—moments, but these torques are relatively low everywhere except in the anterior corpus. In the corpus under the premolars, lateral transverse bending moments and AP twisting moments reach their highest values, approaching the sagittal bending moments in magnitude, which are low in this region of the mandible (Fig. 2).

On the working-side, the AP twisting moments and lateral transverse bending are similar in magnitude to those on the balancing-side, but the sagittal bending moments are lower. Sagittal bending moments, AP twisting moments, and lateral transverse bending moments

all reach similar maxima in the corpus below the bite points (P_3, P_4, and M_1), and lateral transverse shear forces also peak in the anterior corpus. At progressively more posterior sections through the working-side corpus, sagittal bending moments decrease more rapidly than AP torques, so that they are roughly equal in magnitude in the region of M_2, and AP torques are larger than transverse or vertical torques in the corpus below M_3. Sagittal shear is the dominant loading regime behind the bite point (Figs. 2 and 3B). Hylander suggested that biting on the anterior region of the postcanine tooth row (as modeled here) would generate negative AP torques—inverting the base of the mandible—under the bite point, and that muscle forces would generate positive AP torques—everting the base and angle of the ramus (Hylander, 1979c). Our loading and deformation regimes corroborate this hypothesis (Fig. 2; SOM Fig. S6). Examination of the individual torques acting about a frontal section through the mandible below M_1 confirm that bite force contributes significantly to negative AP twisting moments acting on the working-side postcanine corpus. It also reveals powerful negative AP twisting moments generated by vertical components of balancing-side muscle force, previously neglected in discussions of primate mandibular mechanics. The largest negative twisting moments are associated with the vertical and horizontal components of bite force acting on M_1, and the vertical components of balancing-side temporalis and superficial masseter muscle force.

Importantly, our modeling provides new insight into the loading regime of the symphyseal region late in the power stroke. In vivo bone strain recordings from the labial surface of the symphyseal region in macaques suggest that negative frontal shear and/or negative ML twisting are important loading regimes in the symphyseal region (Hylander, 1984). However, it was not possible to discriminate between these loading regimes using in vivo data because it is difficult to record strain from the lingual aspect of the symphyseal region during normal feeding (Hylander, 1979b), and because information on the moments acting about the symphysis has been scant. Our estimates of the loading regime in the symphysis confirm the presence of large negative shearing forces (−30 N) in frontal planes through the symphyseal region (Fig. 3) and our strain data do reveal negative frontal shear strains on the labial surface of the symphysis (Fig. 6). However, analysis of all the moments acting about the symphyseal region reveals that at this time in the power stroke negative ML twisting moments (0.7 Nm) are greater than AP twisting moments (0.4 Nm), and approach lateral transverse bending (wishboning) moments (1.0 Nm) in magnitude (Figs. 2 and 6I–K). The combination of negative AP twisting of both working- and balancing-side mandibles means that the centre of flexure of frontal bending of the symphyseal region is not in the midline (Beecher, 1977; Demes et al., 1984; Wolff, 1984), but is shifted towards the working-side (Korioth and Hannam, 1994; Korioth et al., 1992). Moreover, negative AP twisting of both working- and balancing-side mandibles means that positive frontal shear strain is an important component of symphyseal loading. In sum, the symphyseal region does experience the hypothesized positive frontal bending, albeit with a different center of flexure, and the predominant loading regimes are lateral transverse bending and negative ML twisting.

4.2. Strain regimes

The strain regime in the balancing-side mandible reflects the superposition of sagittal and lateral transverse bending. Tensile AP and ε_1 strains dominate the top of the balancing-side corpus and most of the lingual/medial surface of the corpus and ramus, especially the medial prominence and endocondylar ridge (Figs. 4H, I and 6B), whereas compressive AP and ε_2 strains dominate the lateral/buccal surface of the balancing-side mandible, especially its base (Fig. 4J–L). Negative AP twisting is associated with positive transverse shear strains in the medial prominence, extramolar sulcus and endocondylar ridge, and with negative transverse shear strains in the base of the mandible. High sagittal shearing forces are associated with high magnitude sagittal shear strains on the lateral surface of the balancing-side mandible, at the corpus-ramus junction (extramolar sulcus, external oblique line) and in the ramus in and above the endocondylar ridge.

The strain regime in the working-side mandible is marked by strain magnitudes that are, on average, lower than strain magnitudes on the balancing-side. As on the balancing-side, sagittal shear strains are high in the buccal surface and reflect changing patterns of shear forces (Fig. 5F, G). Sagittal bending is associated with alternating patches of positive and negative AP and principal strains in the alveolar process and mandibular base; similar alternating patches of transverse shear strains are associated with alternating patterns of torsion (Fig. 5C, D). Alternating patches of tension and compression have been shown to characterize the base of FEMs of human and *Alligator* mandibles under unilateral loading (Korioth et al., 1992; Rudderman and Mullen, 1992) and are hypothesized for opossums on the basis of in vivo strain gauge studies (Crompton, 1995). Alternating patterns of shear strain in the basal surface associated with alternating twisting moments have not previously been observed. Our in vivo strain gauge data and strain data from the surface of our model below the posterior tooth row (Panagiotopoulou et al., 2017) are similar to those reported by Hylander (1979c, 1981) from the buccal (summarized in Ross et al., 2016: Fig. 1) and lingual surfaces of the working-side corpus (Dechow and Hylander, 2000): ε_1 is oriented upwards and backwards on the buccal surface and upwards and forwards on the lingual surface.

In the symphyseal region, lateral transverse bending results in high magnitude ε_1 and transverse shear strains lingually and high ε_2 strains labially (Fig. 6B, D, F). However, the combination of lateral transverse bending and negative ML twisting means that these strains are not evenly distributed across the symphyseal region. In association with negative ML twisting, the symphyseal region experiences high magnitude frontal and transverse shear strains of opposite signs in lingual and labial surfaces, strains which reach their peaks in the superior and inferior transverse tori (Fig. 6I–K).

The inaccessibility of the ramus for in vivo strain gage recordings means it has been neglected in most recent work on primate mandible biomechanics; our modeling results suggest that more attention to the ramus is warranted. Our estimates of loading regimes reveal high magnitude shearing forces and moments acting on the rami, and strain magnitudes are also high in some regions of the rami. Both working- and balancing-side rami experience high magnitude ε_1 strains on the front edges, and high ε_2 on the back edges, of the rami associated with the high magnitude negative sagittal bending moments acting in

those coronal planes. On the balancing-side, ε_2 strain magnitudes in the back edge of the ramus are higher than those on the working-side because reaction forces from the temporomandibular joint are higher on the balancing-side. High strain magnitudes are also apparent in the endocondylar ridge and torus triangularis on the medial surface of the balancing-side ramus, including high magnitude AP tensile and ε_1 strains associated with negative sagittal bending, transverse tensile and shear strains on associated with lateral transverse bending, and positive transverse shear strains associated with negative AP torsion (Fig. 4C, H, I). These fields of high magnitude strains in the endocondylar ridge and torus triangularis are posterior continuations of fields of similarly high strains in the lingual face and upper edge of the corpus. We hypothesize that these fields of high magnitude strain extending from the bite point to the balancing-side condyle constitute the primary load path, with torus triangularis and the endocondylar ridge constituting the load path across the ramus.

In modern engineering parlance, the load path is the combination of part(s) of a complex structure—usually the stiffest route—that transfers the majority of the load (force) from the load point (bite point) to the support points (condyles). External ridges of cortical bone and internal ‘trajectories’ of trabecular bone have long been argued to be important pathways for transmission of forces through the mandible, whether from muscle to bite point or from muscle and bite point to the TMJ (Gaspard, 1978; Lenhossek, 1920; Walkhoff, 1902; Weidenreich, 1936). Lenhossek (1920) argued that the external oblique line and the torus triangularis reinforce the ramus and transfer temporalis muscle force to the alveolar process and teeth. Weidenreich (1936: 65–66) proposed that the endocondylar ridge and external oblique lines are “means of transmission of force issuing from the coronoid and condyloid processes” to the corpus, and that the endocoronoid ridge and endocondylar crest are “beams strengthening the bone in that direction on which the strain and force is transmitted from both processes to the body of the jaw”. Weidenreich (1936) further hypothesized that the crista ectocondyloidea performed a similar function on the lateral surface of the ramus. Our modeling reveals that the endocondylar ridge, torus triangularis and external oblique lines are highly strained, suggesting that they do transmit large forces. Thus, one key finding from this study is that the morphology of these features may be informative about strain regimes in the anthropoid mandible during mastication. The same cannot be said for the ectocondyloid crest, which does not experience high strains. This crest likely owes its existence to resorption and thinning of bone in planum triangulare lateralis, rather than to reinforcement for transmission of force. In this regard it is worth noting that the ectocondyloid crest lies below the level of the endocondylar ridge and therefore does not correspond to the ridge’s lateral surface.

It is of interest to compare this concentrated strip of high strain in the macaque mandible with the absence of such paths in crania of primates. As we have discussed elsewhere (Prado et al., 2016), the theory of ‘pillars and buttresses’ in the primate cranium is, with the exception of the anterior pillar, not supported by the available morphological and strain data. The only place where a functional pillar—a strip of highly strained bone extending from the tooth row towards the calvaria—is observed is the anterior pillar in macaques, chimpanzees and some fossil humans (Prado et al., 2016).

4.3. Impact of food mechanical properties and relevance for hominid evolutionary studies

Comparative morphometric studies of the relationship between mandible morphology, feeding behavior and diet have employed measures of corpus and symphyseal morphology with limited success (Daegling, 1990; Daegling, 1992, 2007b; Daegling and Grine, 1991, 2006; Daegling and McGraw, 2000, 2001, 2007; Daegling et al., 2011; Hylander, 1988; Ravosa, 1991, 2000; Ross and Iriarte-Diaz, 2014, 2019a; Taylor, 2002, 2006a, 2006b). Our modeling suggests possible reasons for this. One measure used to make inferences about diet is corpus depth, a measure of resistance to sagittal bending. Under sagittal bending, the principal and axial strains should be highest in the upper and lower surfaces of the mandible; to decrease these strains, all things being equal, the depth of the mandible should be increased. Our analysis confirms that late in the power stroke sagittal bending moments are high on both working and balancing-sides, (higher than both AP twisting and transverse bending moments; Fig. 2), and principal and AP axial strains are high in upper and lower surfaces of the mandible (Fig. 4). Moreover, of all the moments acting on the balancing-side corpus, sagittal bending moments show the largest inter-food differences: nut chewing is associated with higher sagittal bending moments than either dried fruit or grape chewing (Fig. 7). Therefore, it is noteworthy that the largest inter-food differences in AP axial and principal strains are not uniformly seen in the upper and lower surfaces of the corpus (Figs. 9 and 10). Instead, the largest differences in s_1 are seen in a strip running along the medial prominence, across the extramolar sulcus to the external oblique line, and along the medial surface of the endocondylar ridge. If mandible form were to be modified to ameliorate these food-related differences in strain magnitudes, it is not obvious that increases in corpus depth would be the most efficient solution. Adding cortical bone to the inferior border to deepen the corpus would certainly increase the resistance to sagittal bending, decreasing strains in the upper and lower surfaces of the corpus, but this is not where food-related variation in strain magnitudes is greatest. Moreover, if food-related changes in corpus shape were effected by recruiting plasticity mechanisms that use strain magnitude as a trigger (Frost, 2003, 2004), our results suggest these mechanisms would not result in increases in corpus depth, but, rather, increases in size or density of the medial prominence and endocondylar ridge.

The external forces producing sagittal bending moments in the balancing- and working-side mandibles also result in large sagittal shearing forces. These are associated with high magnitude sagittal shear strains in the corpus-ramus junction—recessus mandibulae, extramolar sulcus, external oblique line—on both working and balancing-sides, as well the buccal faces of both corpora (behind the bite point on the working-side; Fig. 4; SOM Fig. S5A–E). These same areas display some of the largest food effects on sagittal shear strains (Fig. 9). In order to increase resistance to these food-related increases in sagittal shearing forces, there is no special advantage to increasing corpus depth to increase resistance to increased sagittal shear; rather, cortical bone thickness can be increased anywhere in frontal sections, but especially in locations where cortical bone thickness is reduced. Measures of cortical bone distribution below M_1 and M_2 in the corpus in several groups of primates reveal no significant differences in the relative contribution of cortical bone area (CBA) to subperiosteal area between extant and fossil hominids, between three species of cercopithecoids with different diets, nor between *Cebus capucinus* and *Sapajus apella*

(Daegling, 1989, 1992, 2002). Based on our loading and strain results, we hypothesize that estimates of CBA at more posterior sections, where shear strains are also high, might yield stronger dietary signals.

Another external measure frequently used to make dietary inferences is corpus breadth, roughly in frontal planes, a measure of resistance to transverse bending and, under some mechanical models, torsion (Daegling and Hylander, 1998). Under lateral transverse bending, high magnitude axial and principal strains in the medial and lateral surfaces can be reduced by increasing beam thickness in transverse planes. High magnitude transverse shear strains can be resisted by increasing the amount of bone in frontal cross-sections. In our model, lateral transverse bending of the balancing-side mandible is indeed associated with high magnitude AP tensile and ε_1 strains along the lingual surface of the corpus, high magnitude AP compressive and ε_2 strains along the buccal surface, and positive transverse shear strain in the medial prominence and endocondylar ridge (Fig. 6B, D). However, as noted above, the greatest inter-food variation in ε_1 is seen in a strip along the lingual surface of the corpus, a strip that lies within the region characterised by high magnitude ε_1: medial prominence, extramolar sulcus, torus triangularis, and endocondylar ridge (Fig. 10A–D). Moreover, food-related differences in loading regimes are associated with increased lateral transverse bending moments, especially anteriorly in the corpus (Fig. 7). If mandible form were to be modified to ameliorate these food-related differences in strain magnitudes, adding cortical bone to the medial prominence would simultaneously increase resistance to transverse bending and reduce strains in highly strained areas. Moreover, if food-related changes in corpus shape were effected by recruiting plasticity mechanisms that use strain magnitude as a trigger (Frost, 2003, 2004), our results suggest these mechanisms would result in increases in size or density of the extramolar sulcus, torus triangularis, and endocondylar ridge.

Corpus breadth is also one of several measures used to estimate the resistance of the corpus to AP twisting or torsion, the other measures including Bredt's formula (Daegling, 1989, 1992, 2002, 2007a; Daegling and Hylander, 1998). It is sometimes assumed that chewing on foods of increased dietary toughness or hardness results in increased torsional stress in the corpus associated with increases in the lateral components of jaw-elevator muscle force and bite force (Bouvier, 1986a, 1986b; Daegling, 1989; Daegling and Grine, 1991; Hylander, 1988; Ravosa, 1991, 1996a, 1996b, 1999, 2000; Taylor, 2002, 2006a, 2006b; Taylor et al., 2008). In our study the largest differences in loading and strain regimes (Figs. 7 and 9) are between nuts (characterized by relatively low toughness and high stiffness) on one hand, and grapes (relatively low toughness and stiffness) and dried fruits (relatively high toughness and low stiffness) on the other. It is noteworthy that AP twisting moments show the lowest differences between foods, especially in the posterior corpus (Fig. 7). Many fossil hominids have very broad corpora under the molars and this has been interpreted as improving resistance to torsional stresses associated with eating tougher, harder foods (Daegling, 1989, 1990, 1992, 2001; Daegling and Grine, 1991, 2006; Hylander, 1988). Our macaque data do not support the hypothesis that increased dietary toughness explains the broad corpora of fossil hominids. We acknowledge that the foods fed to our experimental animals are not the most mechanically challenging foods eaten by primates in the lab (Williams et al., 2005) or in the wild (Coiner-Collier et al., 2016; Dominy et al., 2008; McGraw et al., 2011, 2014;

Vogel et al., 2008; Wright, 2005; Yamashita, 2008) and macaque occlusal morphology differs from that of fossil hominids. Thus, it is possible that our findings for macaques are species-specific. Studies in other primate species relating variation in muscle activity during chewing on different foods to variation in mandibular strain regimes are needed to confirm the differences in inter-food loading regimes observed in this study. As noted elsewhere, posterior displacement of the toothrow relative to the anterior border of the ramus in hominids necessitates broadening of the mandible at the ramus-corpus junction regardless of dietary factors (Daegling and Grine, 1991). Our results suggest that interactions between spatial, dietary, and mechanical factors in this highly strained part of the mandible may be of interest in future studies of hominid feeding adaptations.

In the symphyseal region variables used to infer diet include measures of the distribution of cortical bone, as well as maximum and minimum dimensions, the mechanical meanings of which vary with the orientation of the symphysis (Ravosa, 2000; Daegling, 1992, 2001). In the macaque modeled here, as in many cercopithecine monkeys, the maximum dimension from tooth row (symphysion or infradentale anterior) to the back of the inferior transverse torus is oriented obliquely (at about 45°) to the plane of the postcanine tooth rows. This means that, as in hominids, a large proportion of the symphyseal cross-section is oriented so as to reduce moments and strains associated with transverse bending (Daegling, 2001). Interpreting the mechanical significance of interspecific variation in these measures is complicated by the difficulty of estimating the moments and shear forces acting on the symphyseal region. Our modeling reveals similar magnitudes of food-related variation in AP, SI and ML moments, with the largest differences being in SI—lateral transverse bending—moments (Fig. 7). Our FEM study confirms that the lingual surfaces of the superior and the inferior transverse tori experience the highest ML tensile strains and the highest ε_1 strains, as expected for the concave surfaces of a curved symphyseal region under lateral transverse bending (Hylander, 1984; Fig. 6). Moreover, there is significant food-related variation in ε_1 strain in the posterior surfaces of the superior and (especially) the inferior transverse tori (Figs. 9 and 10). Thus, our empirical findings support the frequent theoretical assumption that measures of symphyseal resistance to lateral transverse bending are good candidates for recovering dietary signals in fossil hominid mandibles. However, lateral transverse bending is not the only important loading regime in the symphyseal region: our modeling results suggests that the ML twisting regime also results in transverse and frontal shear strains on lingual/labial or superior/inferior surfaces of the symphyseal region that equal or exceed those associated with lateral transverse bending (Fig. 6). Food-related variation in ML twisting moments is less than that of lateral transverse bending (Fig. 6), but food-related variation in transverse shear strains in the symphyseal region is significant (Fig. 9Q–T). These results suggest that symphyseal measures that capture resistance to ML twisting, notably the distribution of cortical bone in the symphyseal region, may also be useful for dietary reconstruction in fossil taxa.

One of the most interesting results of our modeling is the observation that these areas of the symphyseal region that experience high magnitude ε_1 and transverse shear strains are continuous with similar areas along the balancing-side mandible—medial prominence, retromolar triangle, extramolar sulcus, torus triangularis, and endocondylar ridge. We suggested above that this strain distribution might indicate that this is the principal load path

from the bite point to the balancing-side condyle. In this context, it is significant that these areas, from symphysis to endocondylar ridge, also manifest the largest variation in maximum principal and transverse shear strain magnitudes, both of which increase in nut chewing compared with dried fruit and grape chewing. With the exception of the superior transverse torus in the symphyseal region, traditional external morphometric measures do not capture variation in morphology in these parts of the mandible. Recent experimental (Ravosa et al., 2007; Terhune et al., 2020) and comparative studies (Coiner-Collier et al., 2018; Giesen et al., 2003a, 2003b, 2004; Giesen and van Eijden, 2000; Giesen et al., 2003c) relating internal morphology of the symphysis and condyle to variation in food material properties suggest that work elsewhere along the load path might be of value. However, optimism that this work will reveal highly specific indicators of feeding on specific foods should be tempered by the fact that the load path does not manifest food-specific variation in principal strain orientation: ε_1 orientation in these areas is largely unaffected by chewing on different foods (Fig. 11). The largest changes in principal strain orientations are instead concentrated under the medial and alveolar prominences and on the front of the condylar neck on the working-side, areas where food-associated variation in strain magnitudes is negligible. Nevertheless, variation in cortical bone distribution and in trabecular size and number (if not orientation) along the load path may also provide information on dietary habits.

The broader relevance of this study, including studies of human evolutionary biomechanics, rests in part on similarities between the loading regime documented here and loading regimes acting on other primate mandibles. Our EMG data document late activity in the balancing-side deep masseter and posterior temporalis, simultaneous with decreasing activity in medial pterygoids and superficial masseters (SOM Fig. S1). A triplet motor pattern is seen late in the power stroke in approximately 54 % of chewing cycles by *Macaca fuscata* and 73 % by *Papio anubis* (see Ram and Ross, 2018), and has been described for humans (Langenbach and Hannam, 1999; Møller, 1966) and *Pan,* albeit at a lower frequency (Ram and Ross, 2018). Our model also resembles finite element models of the human mandible in patterns of deformation—rotation about the bite point, eversion of the balancing-side and inversion of the working-side mandible base—and strain, including AP compressive strains in the alveolar process and AP tensile strains in the base of the mandible under the bite point (Korioth and Versluis, 1997; Rudderman and Mullen, 1992; van Eijden, 2000). This suggests that the results presented here may be relevant to hypotheses of mandible function during a significant proportion of cercopithecine and some hominid chewing cycles. In particular, morphological measures of resistance to lateral transverse bending may provide dietary information, as might detailed studies of trabecular morphology in the transverse tori, medial prominence, torus triangularis and endocondylar ridge.

5. Conclusions

Musculoskeletal and FEM of the macaque mandible during mastication suggest that the most important loading regimes in balancing and working hemimandibles are sagittal bending, sagittal shear and lateral transverse bending, with AP twisting moments being smaller. The largest food-related variation in corpus loading regimes is in sagittal bending

and shear, food-related variation in lateral transverse bending is highest in the anterior corpus: food-related variation in AP twisting of the corpora is minimal. In the symphyseal region lateral transverse bending and negative ML twisting are important loading regimes and both show high levels of food-related variation. Food-related variation in strain regimes is greatest in the lingual symphysis, the balancing-side corpus-ramus junction, and along the balancing-side medial prominence and endocondylar ridge. This includes some areas of traditional focus—lingual symphysis—and areas that have not previously been considered. Specifically, our work highlights the importance of the medial prominence, torus triangularis and endocondylar ridge, and suggests that these may constitute the load path from bite point to balancing-side condyle and ramus.

Supplementary Material

Refer to Web version on PubMed Central for supplementary material.

References

Anapol F, Shahnoor N, Ross CF, 2008 Scaling of reduced physiologic cross-sectional area in primate muscles of mastication In: Vinyard C, Wall CE, Ravosa MJ (Eds.), Primate Craniofacial Function and Biology. Springer, New York, pp. 201–216.

Beecher RM, 1977 Function and fusion at the mandibular symphysis. Am J Phys Anthropol 47, 325–336. [PubMed: 410309]

Bouvier M, 1986a A biomechanical analysis of mandibular scaling in Old World monkeys. Am J Phys Anthropol 69, 473–482.

Bouvier M, 1986b Biomechanical scaling of mandibular dimensions in New World monkeys. Int J Primatol 7, 551–567.

Chalk J, Richmond BG, Ross CF, Strait DS, Wright BW, Spencer MA, Wang Q, Dechow PC, 2011 A finite element analysis of masticatory stress hypotheses. Am J Phys Anthropol 145, 1–10. [PubMed: 21484756]

Coiner-Collier S, Scott RS, Chalk-Wilayto J, Cheyne SM, Constantino P, Dominy NJ, Elgart AA, Glowacka H, Loyola LC, Ossi-Lupo K, Raguet-Schofield M, Talebi MG, Sala EA, Sieradzy P, Taylor AB, Vinyard CJ, Wright BW, Yamashita N, Lucas PW, Vogel ER, 2016 Primate dietary ecology in the context of food mechanical properties. J Hum Evol 98, 103–118. [PubMed: 27542555]

Coiner-Collier S, Vogel ER, Scott RS, 2018 Trabecular anisotropy in the primate mandibular condyle is associated with dietary toughness. Anat Rec 301, 1342–1359.

Crompton AW, 1995 Masticatory function in nonmammalian cynodonts and early mammals In: Thomason JJ (Ed.), Functional Morphology in Vertebrate Paleontology. Cambridge University Press, New York, pp. 55–75.

Daegling DJ, 1989 Biomechanics of cross-sectional size and shape in the hominoid mandibular corpus. Am J Phys Anthropol 80, 91–106. [PubMed: 2508480]

Daegling DJ, 1990 Geometry and biomechanics of hominoid mandibles. Ph.D. Dissertation, State University of New York at Stony Brook.

Daegling DJ, 1992 Mandibular morphology and diet in the genus *Cebus*. Int J Primatol 13, 545–570.

Daegling DJ, 1993 The relationship of in vivo bone strain to mandibular corpus morphology in *Macaca fascicularis*. J Hum Evol 25, 247–269.

Daegling DJ, 2001 Biomechanical scaling of the hominoid mandibular symphysis. J Morphol 250, 12–23. [PubMed: 11599012]

Daegling DJ, 2002 Bone geometry in cercopithecoid mandibles. Arch Oral Biol 47, 315–325. [PubMed: 11922874]

Daegling DJ, 2007a Morphometric estimation of torsional stiffness and strength in primate mandibles. Am J Phys Anthropol 132, 261–266. [PubMed: 17133432]

Daegling DJ, 2007b Relationship of bone utilization and biomechanical competence in hominoid mandibles. Arch Oral Biol 52, 51–63. [PubMed: 17045235]

Daegling DJ, Carlson KJ, Tafforeau P, de Ruiter DJ, Berger LR, 2016 Comparative biomechanics of *Australopithecus sediba* mandibles. J Hum Evol 100, 73–86. [PubMed: 27765151]

Daegling DJ, Grine FE, 1991 Compact bone distribution and biomechanics of early hominid mandibles. Am J Phys Anthropol 86, 321–339. [PubMed: 1746641]

Daegling DJ, Grine FE, 2006 Mandibular biomechanics and the paleontological evidence for the evolution of human diet In: Ungar PS (Ed.), Evolution of the Human Diet: The Known, the Unknown, and the Unknowable. Oxford University Press, Cary, pp. 77–105.

Daegling DJ, Hotzman J, 2003 Functional significance of cortical bone distribution in anthropoid mandibles: An in vitro assessment of bone strain under combined loads. Am J Phys Anthropol 122, 38–50. [PubMed: 12923903]

Daegling DJ, Hylander WL, 1998 Biomechanics of torsion in the human mandible. Am J Phys Anthropol 105, 73–87. [PubMed: 9537929]

Daegling DJ, Hylander WL, 2000 Experimental observation, theoretical models, and biomechanical inference in the study of mandibular form. Am J Phys Anthropol 112, 541–551. [PubMed: 10918128]

Daegling DJ, McGraw WS, 2000 Gnathic morphology and feeding ecology in papionin primates. Am J Phys Anthropol 111 (S30), 134.

Daegling DJ, McGraw WS, 2001 Feeding, diet, and jaw form in West African *Colobus* and *Procolobus*. Int J Primatol 22, 1033–1055.

Daegling DJ, McGraw WS, 2007 Functional morphology of the mangabey mandibular corpus: Relationship to dental specializations and feeding behavior. Am J Phys Anthropol 134, 50–62. [PubMed: 17503450]

Daegling DJ, McGraw WS, Ungar PS, Pampush JD, Vick AE, Bitty EA, 2011 Hard-object feeding in sooty mangabeys (Cercocebus atys) and interpretation of early hominin feeding ecology. PLoS One 6, e23095. [PubMed: 21887229]

Daegling DJ, Ravosa MJ, Johnson KR, Hylander WL, 1992 Influence of teeth, alveoli, and periodontal ligaments on torsional rigidity in human mandibles. Am J Phys Anthropol 89, 59–72. [PubMed: 1530062]

Dechow PC, Hylander WL, 2000 Elastic properties and masticatory bone stress in the macaque mandible. Am J Phys Anthropol 112, 541–552. [PubMed: 10918128]

Dechow PC, Panagiotopoulou O, Gharpure P, 2017 Biomechanical implications of cortical elastic properties of the macaque mandible. Zoology (Jena) 124, 3–12. [PubMed: 28811166]

Demes B, Preuschoft H, Wolff JEA, 1984 Stress-strength relationship in the mandible of hominoids In: Chivers D, Wood B, Bilsborough A (Eds.), Food Acquisition and Processing in Primates. Plenum Press, New York, pp. 369–390.

Dominy NJ, Vogel ER, Yeakel JD, Constantino P, Lucas PW, 2008 Mechanical properties of plant underground storage organs and implications for dietary models of early hominins. Evol Biol 35, 159–175.

Frost HM, 2003 Bone's mechanostat: a 2003 update. Anat Rec 275, 1081–1101.

Frost HM, 2004 A 2003 update of bone physiology and Wolff's Law for clinicians. Angle Orthod 74, 3–15. [PubMed: 15038485]

Gaspard M, 1978 L'appareil Manducateur et la Manducation. Anatomie Descriptive, Ontogenèse et Phylogenèse de la Mandibule Humaine Première Partie, Volume 1 J. Prélat, Paris.

Giesen EB, Ding M, Dalstra M, van Eijden TM, 2003a Architectural measures of the cancellous bone of the mandibular condyle identified by principal components analysis. Calcif Tissue Int 73, 225–231. [PubMed: 14667134]

Giesen EB, Ding M, Dalstra M, van Eijden TM, 2003b Reduced mechanical load decreases the density, stiffness, and strength of cancellous bone of the mandibular condyle. Clin Biomech 18, 358–363.

Giesen EB, Ding M, Dalstra M, van Eijden TM, 2004 Changed morphology and mechanical properties of cancellous bone in the mandibular condyles of edentate people. J Dent Res 83, 255–259. [PubMed: 14981130]

Giesen EB, van Eijden TM, 2000 The three-dimensional cancellous bone architecture of the human mandibular condyle. J Dent Res 79, 957–963. [PubMed: 10831098]

Giesen EBW, Ding M, Dalstra M, van Eijden TMGJ, 2003c Reduced mechanical load decreases the density, stiffness, and strength of cancellous bone of the mandibular condyle. Clin Biomech 18, 358–363.

Grine FE, Judex S, Daegling DJ, Ozcivici E, Ungar PS, Teaford MF, Sponheimer M, Scott J, Scott RS, Walker A, 2010 Craniofacial biomechanics and functional and dietary inferences in hominin paleontology. J Hum Evol 58, 293–308. [PubMed: 20227747]

Grőning F, Fagan M, O'Higgins P, 2012 Modeling the human mandible under masticatory loads: which input variables are important? Anat Rec 295, 853–863.

Hibbeler RC, 2000 Mechanics of Materials. Prentice Hall, Upper Saddle River, New Jersey.

Hylander WL, 1977 In vivo bone strain in the mandible of *Galago crassicaudatus*. Am J Phys Anthropol 46, 309–326. [PubMed: 403774]

Hylander WL, 1979a An experimental analysis of temporomandibular joint reaction force in macaques. Am J Phys Anthropol 51, 433–456. [PubMed: 532828]

Hylander WL, 1979b The functional significance of primate mandibular form. J Morphol 160, 223–240. [PubMed: 458862]

Hylander WL, 1979c Mandibular function in *Galago crassicaudatus* and *Macaca fascicularis*: An in vivo approach to stress analysis of the mandible. J Morphol 159, 253–296. [PubMed: 105147]

Hylander WL, 1981 Patterns of stress and strain in the macaque mandible In: Carlson DS (Ed.), Craniofacial Biology. University of Michigan, Ann Arbor, pp. 1–35.

Hylander WL, 1984 Stress and strain in the mandibular symphysis of primates: A test of competing hypotheses. Am J Phys Anthropol 64, 1–46. [PubMed: 6731608]

Hylander WL, 1985 Mandibular function and biomechanical stress and scaling. Am Zool 25, 315–330.

Hylander WL, 1986 In vivo bone strain as an indicator of masticatory bite force in *Macaca fascicularis*. Arch. Oral Biol 31, 149–157. [PubMed: 3459403]

Hylander WL, 1988 Implications of in vivo experiments for interpreting the functional significance of "robust" australopithecine jaws In: Grine FE (Ed.), Evolutionary History of the "Robust" Australopithecines. Aldine de Gruyter, New York, pp. 55–83.

Hylander WL, Crompton AW, 1986 Jaw movements and patterns of mandibular bone strain during mastication in the monkey *Macaca fascicularis*. Arch Oral Biol. 31, 841–848. [PubMed: 3479960]

Hylander WL, Johnson KR, 1989 The relationship between masseter force and masseter electromyogram during mastication in the monkey *Macaca fascicularis*. Arch Oral Biol 34, 713–722. [PubMed: 2624563]

Hylander WL, Johnson KR, 1993 Modeling relative masseter force from surface electromyograms during mastication in non-human primates. Arch Oral Biol 38, 233–240. [PubMed: 8489417]

Hylander WL, Johnson KR, 1994 Jaw muscle function and wishboning of the mandible during mastication in macaques and baboons. Am J Phys Anthropol 94, 523–547. [PubMed: 7977678]

Hylander WL, Johnson KR, 1997 In vivo bone strain patterns in the zygomatic arch of macaques and the significance of these patterns for functional interpretations of craniofacial form. Am J Phys Anthropol 102, 203–232. [PubMed: 9066901]

Hylander WL, Johnson KR, Crompton AW, 1987 Loading patterns and jaw movements during mastication in *Macaca fascicularis*: A bone-strain, electromyographic, and cineradiographic analysis. Am J Phys Anthropol 72, 287–314. [PubMed: 3578494]

Hylander WL, Picq PG, Johnson KR, 1991 Masticatory-stress hypotheses and the supraorbital region of primates. Am J Phys Anthropol 86, 1–36. [PubMed: 1951658]

Hylander WL, Ravosa MJ, Ross CF, 2004 Jaw muscle recruitment patterns during mastication in anthropoids and prosimians In: Anapol F, German RZ, Jablonski NG (Eds.), Shaping Primate Evolution. Cambridge University Press, Cambridge, pp. 229–257.

Hylander WL, Ravosa MJ, Ross CF, Johnson KR, 1998 Mandibular corpus strain in Primates: Further evidence for a functional link between symphyseal fusion and jaw-adductor muscle force. Am J Phys Anthropol 107, 257–271. [PubMed: 9821491]

Hylander WL, Ravosa MJ, Ross CF, Wall CE, Johnson KR, 2000 Symphyseal fusion and jaw-adductor muscle force: An EMG study. Am J Phys Anthropol 112, 469–492. [PubMed: 10918125]

Hylander WL, Vinyard CJ, Wall CE, Williams SH, Johnson KR, 2002 Recruitment and firing patterns of jaw muscles during mastication in ring-tailed lemurs. Am J Phys Anthropol 117 (S34), 88.

Hylander WL, Vinyard CJ, Wall CE, Williams SH, Johnson KR, 2011 Functional and evolutionary significance of the recruitment and firing patterns of the jaw adductors during chewing in verreaux's sifaka (*Propithecus verreauxi*). Am J Phys Anthropol 145, 531–547. [PubMed: 21590749]

Hylander WL, Wall CE, Vinyard CJ, Ross C, Ravosa MR, Williams SH, Johnson KR, 2005 Temporalis function in anthropoids and strepsirrhines: An EMG study. Am J Phys Anthropol 128, 35–56. [PubMed: 15714512]

Keiter F, 1935 An anthropological study of the Schwaebische Alb Mountain Range Region. Petermanns Mitt 81, 254–254.

Korioth TW, Hannam AG, 1994 Deformation of the human mandible during simulated tooth clenching. J Dent Res 73, 56–66. [PubMed: 8294619]

Korioth TW, Romilly DP, Hannam AG, 1992 Three-dimensional finite element stress analysis of the dentate human mandible. Am J Phys Anthropol 88, 69–96. [PubMed: 1510115]

Korioth TW, Versluis A, 1997 Modeling the mechanical behavior of the jaws and their related structures by finite element (FE) analysis. Crit. Rev. Oral. Biol. Med 8, 90–104. [PubMed: 9063627]

Langenbach GEJ, Hannam AG, 1999 The role of passive muscle tensions in a three-dimensional dynamic model of the human jaw. Arch Oral Biol 44, 557–573. [PubMed: 10414871]

Ledogar JA, Smith AL, Benazzi S, Weber GW, Spencer MA, Carlson KB, McNulty KP, Dechow PC, Grosse IR, Ross CF, Richmond BG, Wright BW, Wang Q, Byron C, Carlson KJ, de Ruiter DJ, Berger LR, Tamvada K, Pryor LC, Berthaume MA, Strait DS, 2016 Mechanical evidence that *Australopithecus sediba* was limited in its ability to eat hard foods. Nat Commun 7, 10596. [PubMed: 26853550]

Lenhossek M.v., 1920 Das innere Relief des Unterkieferasten. Arch. Anthropol 18, 49–59.

Lieberman DE, Ross CF, Ravosa MJ, 2000 The primate cranial base: ontogeny, function, and integration. Yearb. Phys. Anthropol 43, 117–169.

McGraw WS, Daegling DJ, 2012 Primate feeding and foraging: Integrating studies of behavior and morphology. Annu. Rev. Anthropol 41, 203–219.

McGraw WS, Daegling DJ, 2020 Diet, feeding behavior, and jaw architecture of Tai monkeys: Congruence and chaos in the realm of functional morphology. Evol Anthropol. 29, 14–28. [PubMed: 31580522]

McGraw WS, Vick AE, Daegling DJ, 2011 Sex and age differences in the diet and ingestive behaviors of Sooty Mangabeys (*Cercocebus atys*) in the Tai Forest, Ivory Coast. Am J Phys Anthropol 144, 140–153. [PubMed: 20925080]

McGraw WS, Vick AE, Daegling DJ, 2014 Dietary variation and food hardness in Sooty Mangabeys (*Cercocebus atys*): Implications for fallback foods and dental adaptation. Am J Phys Anthropol 154, 413–423. [PubMed: 24810136]

Mehari Abraha H, Iriarte-Diaz J, Ross CF, Taylor AB, Panagiotopoulou O, 2019 The mechanical effect of the periodontal ligament on bone strain regimes in a validated finite element model of a macaque mandible. Front. Bioeng. Biotech 7, 269.

Mendez J, Keys A, 1960 Density and composition of mammalian muscle. Metabolism 9, 184–188.

Moazen M, Curtis N, O'Higgins P, Evans SE, Fagan MJ, 2009 Biomechanical assessment of evolutionary changes in the lepidosaurian skull. Proc Natl Acad Sci U S A 106, 8273–8277. [PubMed: 19416822]

Møller E, 1966 The chewing apparatus. An electromyographic study of the action of the muscles of mastication and its correlation to facial morphology. Acta Physiol Scand 69 (Suppl. 280), 1–229.

Panagiotopoulou O, Iriarte-Diaz J, Wilshin S, Dechow PC, Taylor AB, Mehari Abraha H, Aljunid SF, Ross CF, 2017 In vivo bone strain and finite element modeling of a rhesus macaque mandible during mastication. Zoology 124, 13–29. [PubMed: 29037463]

Piveteau J, 1957 Traité de Paléontologie, Volume 7, Primates: Paléontologie Humaine Masson, Paris.

Porro LB, Holliday CM, Anapol F, Ontiveros LC, Ontiveros LT, Ross CF, 2011 Free body analysis, beam mechanics, and finite element modeling of the mandible of *Alligator mississippiensis*. J Morphol 272, 910–937. [PubMed: 21567445]

Porro LB, Metzger K, Iriarte-Diaz J, Ross CF, 2013 In vivo bone strain and finite element modeling of the mandible of *Alligator mississippiensis*. Journal of Anatomy 223, 195–227. [PubMed: 23855772]

Prado FB, Freire AR, Claudia Rossi A, Ledogar JA, Smith AL, Dechow PC, Strait DS, Voigt T, Ross CF, 2016 Review of in vivo bone strain studies and finite element models of the zygomatic complex in humans and nonhuman primates: Implications for clinical research and practice. Anat Rec 299, 1753–1778.

Rak Y, 1983 The Australopithecine Face. Academic Press, New York.

Ram Y, Ross CF, 2018 Evaluating the triplet hypothesis during rhythmic mastication in Primates. J Exp Biol 221, jeb165985.

Rasche W, 1913 Beiträge zur Anthropologie des Unterkiefers. Kgl. Hof- und Univ.-Buchdr. Dr. C Wolf & Sohn, München. .

Ravosa MJ, 1988 Browridge development in Cercopithecidae: A test of two models. Am J Phys Anthropol 76, 535–555.

Ravosa MJ, 1991 Structural allometry of the mandibular corpus and symphysis in prosimian primates. J Hum Evol 20, 3–20.

Ravosa MJ, 1996a Jaw morphology and function in living and fossil Old World Monkeys. Int J Primatol 17, 909–932.

Ravosa MJ, 1996b Mandibular form and function in North American and European Adapidae and Omomyidae. J Morphol 229, 171–190. [PubMed: 8755338]

Ravosa MJ, 1999 Anthropoid origins and the modern symphysis. Folia Primatol 70, 65–78. [PubMed: 10085514]

Ravosa MJ, 2000 Size and scaling in the mandible of living and extinct apes. Folia Primatol 71, 305–322. [PubMed: 11093035]

Ravosa MJ, Hogue A, 2004 Function and fusion of the mandibular symphysis in mammals: a comparative and experimental perspective In: Ross CF, Kay RF (Eds.), Anthropoid Origins: New Visions. Kluwer Academic/Plenum Publishers, New York, pp. 413–462.

Ravosa MJ, Kunwar R, Stock SR, Stack MS, 2007 Pushing the limit: masticatory stress and adaptive plasticity in mammalian craniomandibular joints. J Exp Biol 210, 628–641. [PubMed: 17267649]

Ravosa MJ, Menegaz RA, Scott JE, Daegling DJ, McAbee KR, 2016 Limitations of a morphological criterion of adaptive inference in the fossil record. Biol Rev 91, 883–898. [PubMed: 26052620]

Ravosa MJ, Simons EL, 1994 Mandibular growth and function in *Archaeolemur*. Am J Phys Anthropol 95, 63–76. [PubMed: 7998602]

Ravosa MJ, Vinyard CJ, Gagnon M, Islam SA, 2000 Evolution of anthropoid jaw loading and kinematic patterns. Am J Phys Anthropol 112, 493–516. [PubMed: 10918126]

Rayfield EJ, 2011 Strain in the ostrich mandible during simulated pecking and validation of specimen-specific finite element models. Journal of Anatomy 218, 47–58. [PubMed: 20846282]

Reed DA, Ross CF, 2010 The influence of food material properties on jaw kinematics in the primate, *Cebus*. Arch. Oral Biol 55, 946–962. [PubMed: 20880517]

Rightmire GP, Deacon HJ, 1991 Comparative studies of Late Pleistocene human remains from Klasies River Mouth, South Africa. J Hum Evol 20, 131–156.

Robinson JT, 1972 Early Hominid Posture and Locomotion. University of Chicago Press, Chicago.

Ross CF, Berthaume MA, Dechow PC, Iriarte-Diaz J, Porro LB, Richmond BG, Spencer M, Strait D, 2011 *In vivo* bone strain and finite-element modeling of the craniofacial haft in catarrhine primates. J. Anat 218, 112–148. [PubMed: 21105871]

Ross CF, Iriarte-Diaz J, 2014 What does feeding system morphology tell us about feeding? Evol. Anthropol 23, 105–120. [PubMed: 24954218]

Ross CF, Iriarte-Diaz J, 2019 Evolution, constraint and optimality in primate feeding systems In: Bels V, Whishaw IQ (Ed.), Feeding in Vertebrates. Springer, Cham, pp. 787–828.

Ross CF, Iriarte-Diaz J, Nunn CL, 2012 Innovative approaches to the relationship between diet and mandibular morphology in primates. Int J Primatol 33, 632–660.

Ross CF, Washington RL, Eckhardt A, Reed DA, Vogel ER, Dominy NJ, Machanda ZP, 2009 Ecological consequences of scaling of chew cycle duration and daily feeding time in Primates. J Hum Evol 56, 570–585. [PubMed: 19447470]

Rudderman RH, Mullen RL, 1992 Biomechanics of the facial skeleton. Clin. Plast. Surg 19, 11–29. [PubMed: 1537212]

Scott RS, Ungar PS, Bergstrom TS, Brown CA, Grine FE, Teaford MF, Walker A, 2005 Dental microwear texture analysis shows within-species diet variability in fossil hominins. Nature 436, 693–695. [PubMed: 16079844]

Shahnoor S, 2004 Morphological adaptations to diet in primate masticatory muscles. Ph.D. Dissertation, University of Wisconsin-Milwaukee.

Sinclair AG, Alexander RM, 1987 Estimated forces exerted by the jaw muscles of some reptiles. J. Zool 213, 107–115.

Smith AL, Benazzi S, Ledogar JA, Tamvada K, Pryor Smith LC, Weber GW, Spencer MA, Dechow PC, Grosse IR, Ross CF, Richmond BG, Wright BW, Wang Q, Byron C, Slice DE, Strait DS, 2015a Biomechanical implications of intraspecific shape variation in chimpanzee crania: moving toward an integration of geometric morphometrics and finite element analysis. Anat Rec 298, 122–144.

Smith AL, Benazzi S, Ledogar JA, Tamvada K, Pryor Smith LC, Weber GW, Spencer MA, Lucas PW, Michael S, Shekeban A, Al-Fadhalah K, Almusallam AS, Dechow PC, Grosse IR, Ross CF, Madden RH, Richmond BG, Wright BW, Wang Q, Byron C, Slice DE, Wood S, Dzialo C, Berthaume MA, van Casteren A, Strait DS, 2015b The feeding biomechanics and dietary ecology of *Paranthropus boisei*. Anat Rec 298, 145–167.

Spears IR, Macho GA, 1998 Biomechanical behaviour of modern human molars: Implications for interpreting the fossil record. Am J Phys Anthropol 106, 467–482. [PubMed: 9712476]

Strait D, Richmond BG, Spencer M, Ross CF, Wood B, 2007 Something to chew on: Masticatory biomechanics and its relevance to early hominid phylogeny. J Hum Evol 52, 585–599. [PubMed: 17386938]

Strait D, Wang Q, Dechow PC, Ross CF, Richmond B, Spencer M, Patel BA, 2005 Modeling elastic properties in finite element analysis: how much precision is needed to produce an accurate model? Anat. Rec 283A, 275–287.

Strait DS, Constantino P, Lucas PW, Richmond BG, Spencer MA, Dechow PC, Ross CF, Grosse IR, Wright BW, Wood BA, Weber GW, Wang Q, Byron C, Slice DE, Chalk J, Smith AL, Smith LC, Wood S, Berthaume M, Benazzi S, Dzialo C, Tamvada K, Ledogar JA, 2013 Viewpoints: diet and dietary adaptations in early hominins: the hard food perspective. Am J Phys Anthropol 151, 339–355. [PubMed: 23794330]

Strait DS, Grosse IR, Dechow PC, Smith AL, Wang Q, Weber GW, Neubauer S, Slice DE, Chalk J, Richmond BG, Lucas PW, Spencer MA, Schrein C, Wright BW, Byron CD, Ross CF, 2010 The structural rigidity of the cranium of *Australopithecus africanus*: Implications for diet, dietary adaptations, and the allometry of feeding biomechanics. Anat. Rec 293, 583–593.

Strait DS, Weber GW, Neubauer S, Chalk J, Richmond BG, Lucas PW, Spencer MA, Schrein C, Dechow PC, Ross CF, Grosse IR, Wright BW, Constantino P, Wood BA, Lawn B, Hylander WL, Wang Q, Byron C, Slice DE, Smith AL, 2009 The feeding biomechanics and dietary ecology of *Australopithecus africanus*. Procc Natl Acad Sci USA 106, 2124–2129.

Taylor AB, 2002 Masticatory form and function in the African apes. Am J Phys Anthropol 117, 133–156. [PubMed: 11815948]

Taylor AB, 2005 A comparative analysis of temporomandibular joint morphology in the African apes. J Hum Evol 48, 555–574. [PubMed: 15927660]

Taylor AB, 2006a Diet and mandibular morphology in African apes. Int J Primatol 27, 181–201.

Taylor AB, 2006b Feeding behavior, diet, and the functional consequences of jaw form in orangutans, with implications for the evolution of *Pongo*. J Hum Evol 50, 377–393. [PubMed: 16413045]

Taylor AB, Eng CM, Anapol FC, Vinyard CJ, 2009 The functional correlates of jaw-muscle fiber architecture in tree-gouging and nongouging callitrichid monkeys. Am J Phys Anthropol 139, 353–367. [PubMed: 19140215]

Taylor AB, Vinyard CJ, 2009 Jaw-muscle fiber architecture in tufted capuchins favors generating relatively large muscle forces without compromising jaw gape. J Hum Evol 57, 710–720. [PubMed: 19875148]

Taylor AB, Vinyard CJ, 2013 The relationships among jaw-muscle fiber architecture, jaw morphology and feeding behavior in extant apes and modern humans. Am J Phys Anthropol 151, 120–134. [PubMed: 23553609]

Taylor AB, Vogel ER, Dominy NJ, 2008 Food material properties and mandibular load resistance abilities in large-bodied hominoids. J Hum Evol 55, 604–616. [PubMed: 18656244]

Taylor AB, Yuan T, Ross CF, Vinyard CJ, 2015 Jaw-muscle force and excursion scale with negative allometry in platyrrhine primates. Am J Phys Anthropol 158, 242–256. [PubMed: 26175006]

Terhune CE, Sylvester AD, Scott JE, Ravosa MJ, 2020 Internal architecture of the mandibular condyle of rabbits is related to dietary resistance during growth. J Exp Biol. 10.1242/jeb.220988

Ungar PS, Grine FE, Teaford MF, 2008 Dental microwear and diet of the Plio-Pleistocene hominin *Paranthropus boisei*. PLoS One 3, e2044. [PubMed: 18446200]

van Eijden TM, 2000 Biomechanics of the mandible. Crit. Rev. Oral. Biol. Med 11, 123–136. [PubMed: 10682903]

Vinyard CJ, Ravosa MJ, 1998 Ontogeny, function, and scaling of the mandibular symphysis in papionin primates. J Morphol 235, 157–175. [PubMed: 9438974]

Virchow H, 1916 Zahnbogen und Alveolarbogen. Z Ethnol 48, 277–295.

Virchow H, 1920 Die menschlichen Skeletreste aus dem Kampfe'schen Bruch im Travertin von Ehringsdorf bei Weimar. Verlag von Gustav Fischer, Jena.

Vogel ER, van Woerden JT, Lucas PW, Atmoko SSU, van Schaik CP, Dominy NJ, 2008 Functional ecology and evolution of hominoid molar enamel thickness: *Pan troglodytes schweinfurthii* and *Pongopygmaeus wurmbii*. J Hum Evol 55, 60–74. [PubMed: 18243275]

Vogel ER, Zulfa A, Hardus ME, Wich SA, Dominy NJ, Taylor AB, 2014 Food mechanical properties, feeding ecology, and the mandibular morphology of wild orangutans. J Hum Evol 75, 110–124. [PubMed: 25038032]

Walkhoff O, 1902 Der Unterkiefer des Anthropomorphen und des Menschen in seiner funktionellen Entwickelung und Gestalt. C. W. Kreidel's Verlag, Wiesbaden.

Weidenreich F, 1936 The mandibles of *Sinanthropus pekinensis:* A comparative study. Palaeontologica Sinica 7, 1–162.

Weijs WA, 1980 Biomechanical models and the analysis of form: a study of the mammalian masticatory apparatus. Am. Zool 20, 707–719.

Weijs WA, Dantuma R, 1975 Electromyography and mechanics of mastication in the albino rat. J Morphol 146, 1–34. [PubMed: 1171253]

Weijs WA, Dantuma R, 1981 Functional anatomy of the masticatory apparatus in the rabbit (*Oryctolagus cuniculus* L.). Neth J Zool 31, 99–147.

Weijs WA, Van der Wielen-Drent TK, 1982 Sarcomere length and EMG activity in some jaw muscles of the rabbit. Acta Anat 113, 178–188. [PubMed: 7124331]

Weijs WA, Van Ruijven LJ, 1990 Models of masticatory mechanics: Their reliability, resolving power and usefulness in functional morphology. Neth J Zool 40, 136–152.

White TD, Black MT, Folkens PA, 2012 Skull: Cranium and Mandible In: White TD, Black MT, Folkens PA (Eds.), Human Osteology, 3rd ed. Academic Press, San Diego, pp. 43–100.

Williams SH, Wright BW, Truong V, Daubert CR, Vinyard CJ, 2005 Mechanical properties of foods used in experimental studies of primate masticatory function. Am J Primatol 67, 329–346. [PubMed: 16287104]

Wolff JEA, 1984 A theoretical approach to solve the chin problem In: Chivers D, Wood B, Bilsborough A (Eds.), Food Acquisition and Processing in Primates. Plenum, New York, pp. 391–405.

Wolpoff MH, 1980 Paleoanthropology. Alfred A. Knopf, New York.

Wright BW, 2005 Craniodental biomechanics and dietary toughness in the genus *Cebus*. J Hum Evol 48, 473–492. [PubMed: 15857651]

Wroe S, Moreno K, Clausen P, McHenry C, Curnoe D, 2007 High-resolution three-dimensional computer simulation of hominid cranial mechanics. Anatomical Record. 290, 1248–1255.

Yamashita N, 2008 Food physical properties and their relationship to morphology: The curious case of *kily* In: Vinyard C, Ravosa MJ, Wall CE (Eds.), Primate Craniofacial Function and Biology. Springer, New York, pp. 387–406.

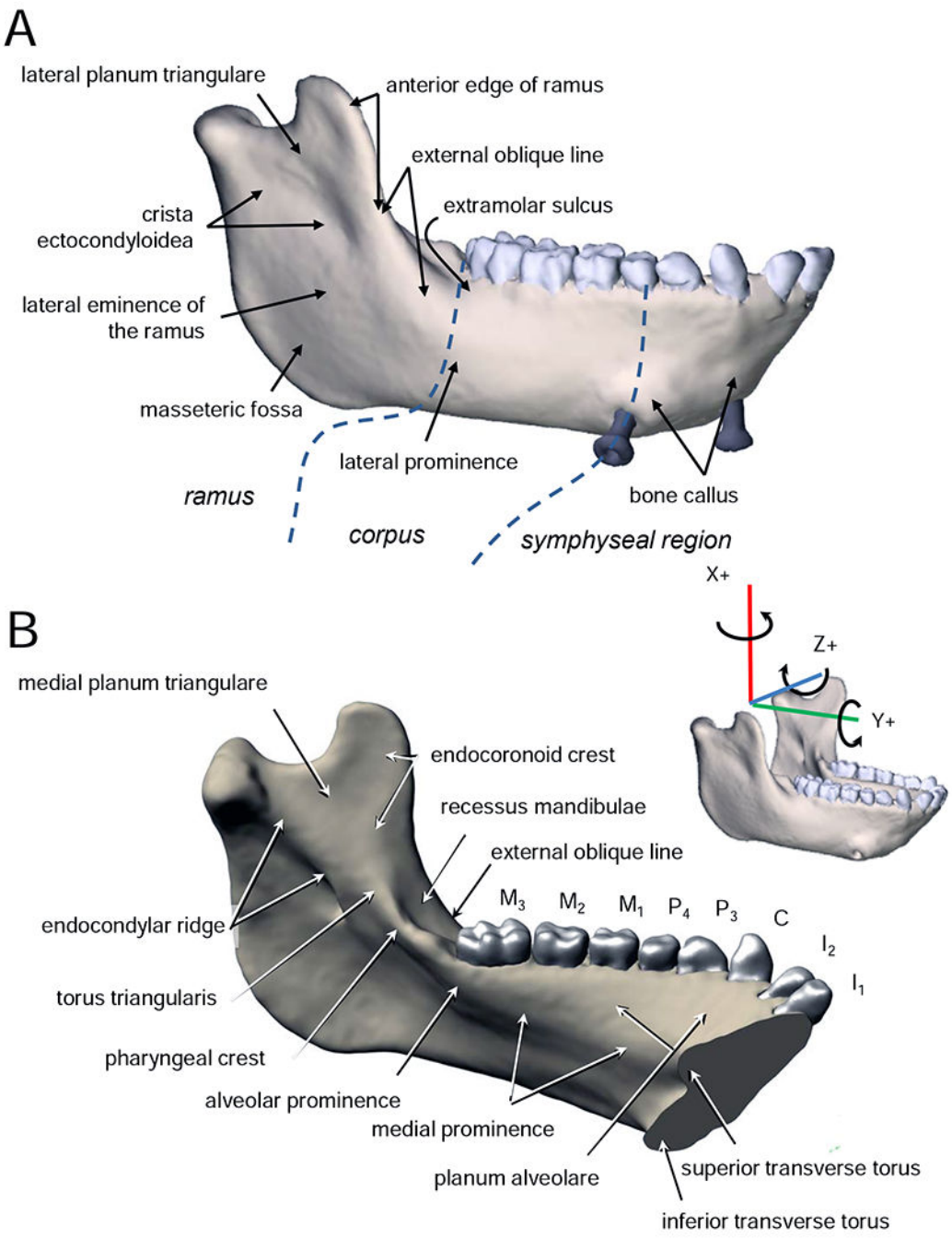

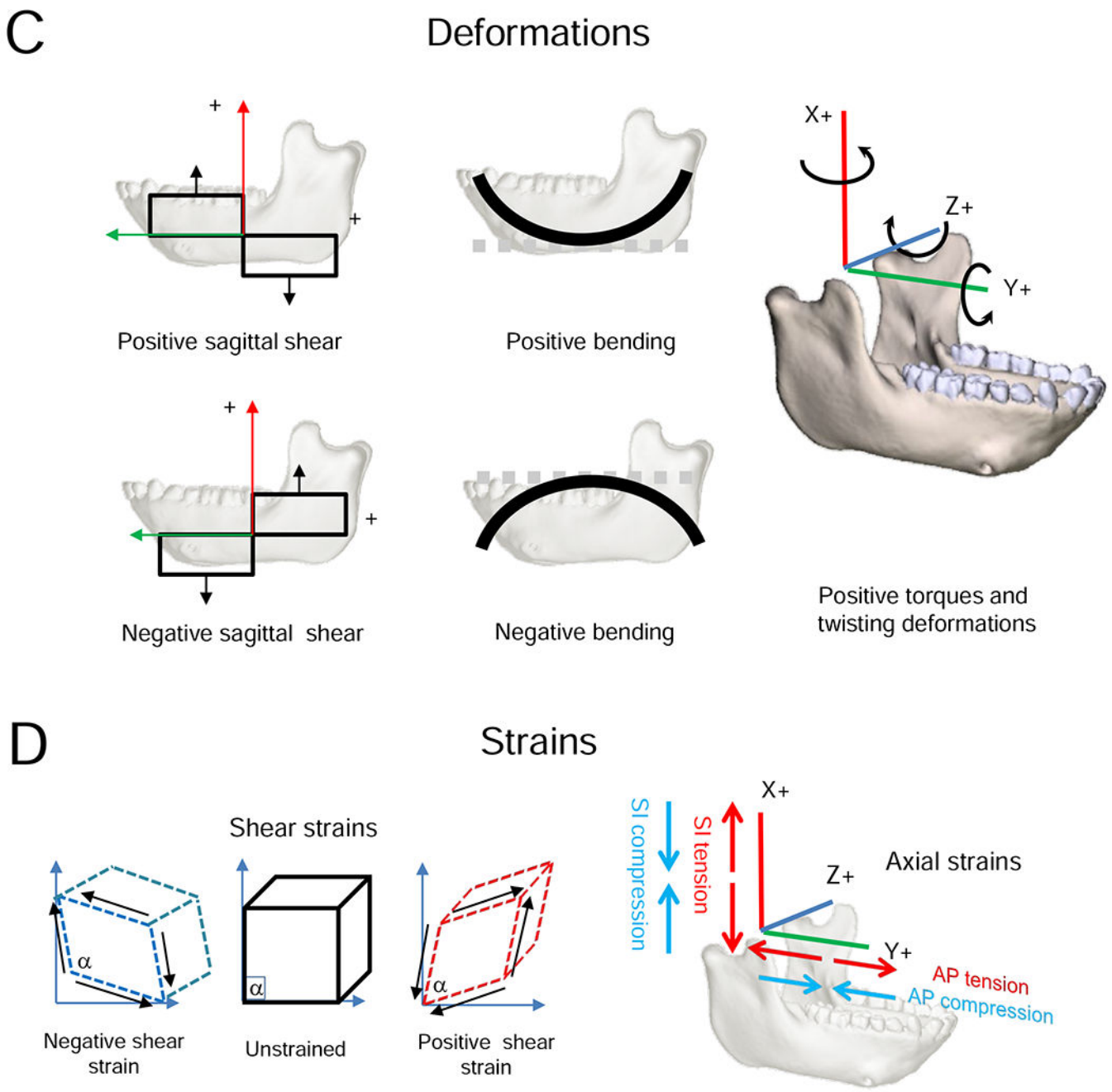

Figure 1.

A) and B) Terminology used in this paper. C, D) Coordinate system and conventions for strain and deformation regimes.

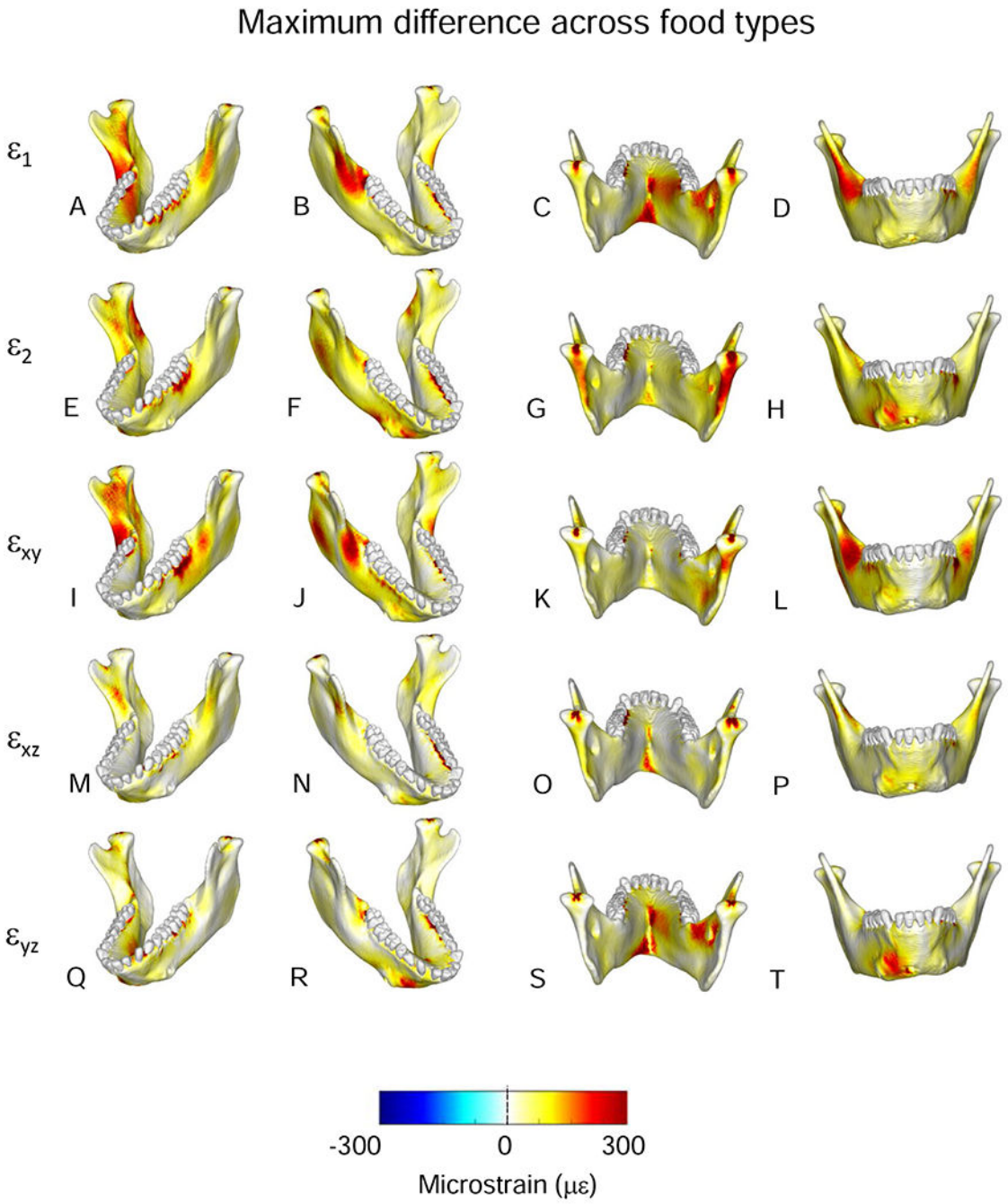

Figure 2.

Moments (in N m) = (force [N] × distance [m]) acting about axes parallel to the coordinate system on the working-side, the balancing-side and through the symphyseal region. Numbers on the ordinate correspond to section planes illustrated in the figures at bottom. Moments about X axes are SI moments (i.e., moments about SI axes), or transverse bending moments (i.e., moments that bend in transverse planes); moments about Y axes are AP or twisting moments; moments about Z are ML or sagittal bending moments. Balancing-side frontal and working-side frontal: These moments are calculated as the sums of all the

moments acting on the bone anterior to frontal planes through the illustrated sections. This includes those moments acting on the contralateral hemi-mandible, whether behind or in front of the section plane. Symphysis frontal: moments about frontal planes through the symphyseal region summed anterior to the illustrated sections. Symphysis sagittal: moments about sagittal planes through the symphyseal region summed to the right of the illustrated sections. For example, moments acting on the midsagittal plane are the sum of all balancing-side moments.

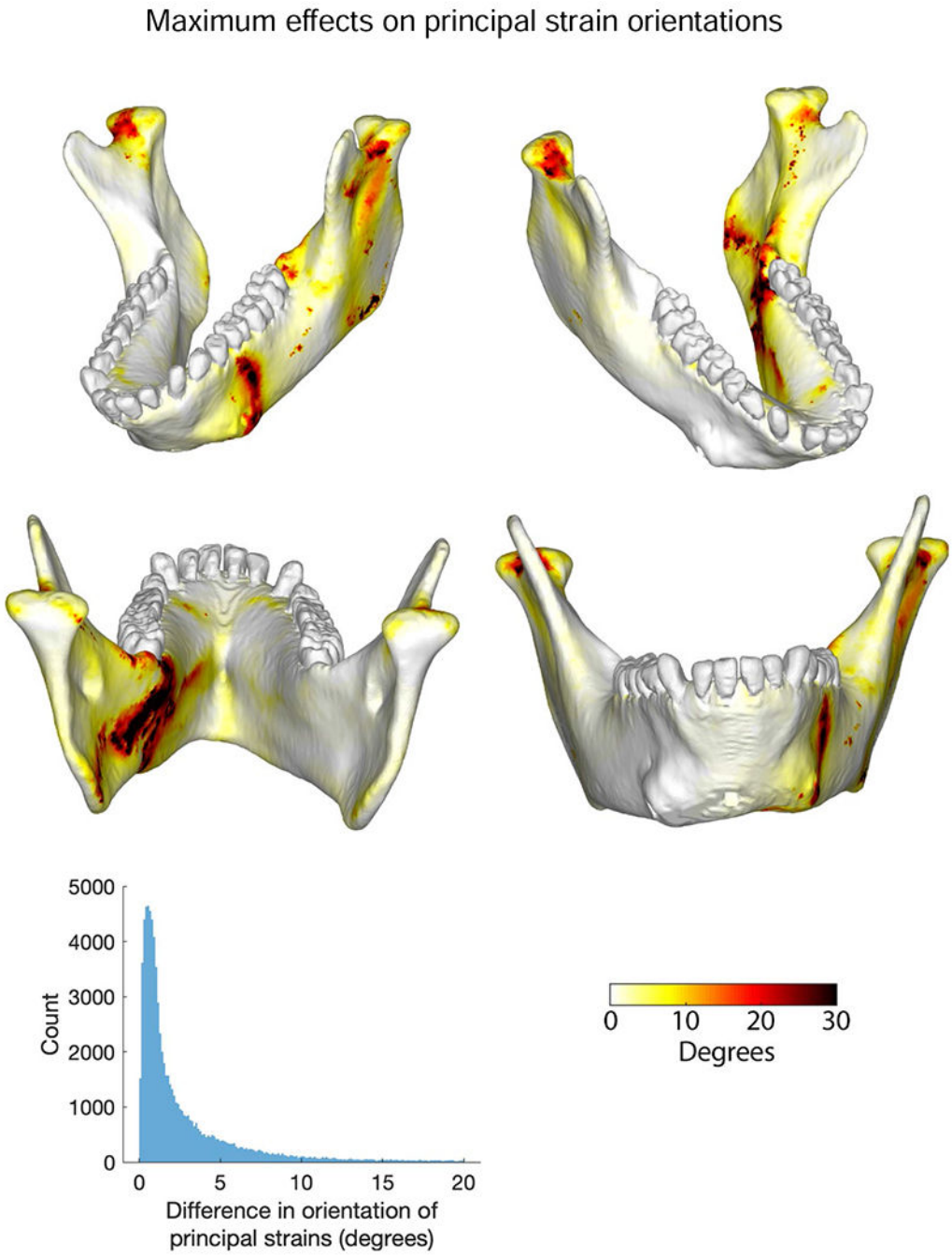

Figure 3.

Shear forces in Newtons (N) acting within specified planes. Sagittal and transverse shear forces are sums of all forces anterior to each coronal plane. Frontal shear forces are sums of all forces to one side of the specified plane. Images of mandible model are aligned to planes for which forces were calculated. A) Working-side vertical, sagittal plane shear forces. B) Working-side transverse plane shear forces. C) Balancing-side vertical, sagittal-plane shear forces. D) Balancing-side transverse plane shear forces. E) Frontal shear forces plotted against mandible width. Key in bottom right illustrates polarity of shear (cf. Fig. 1).

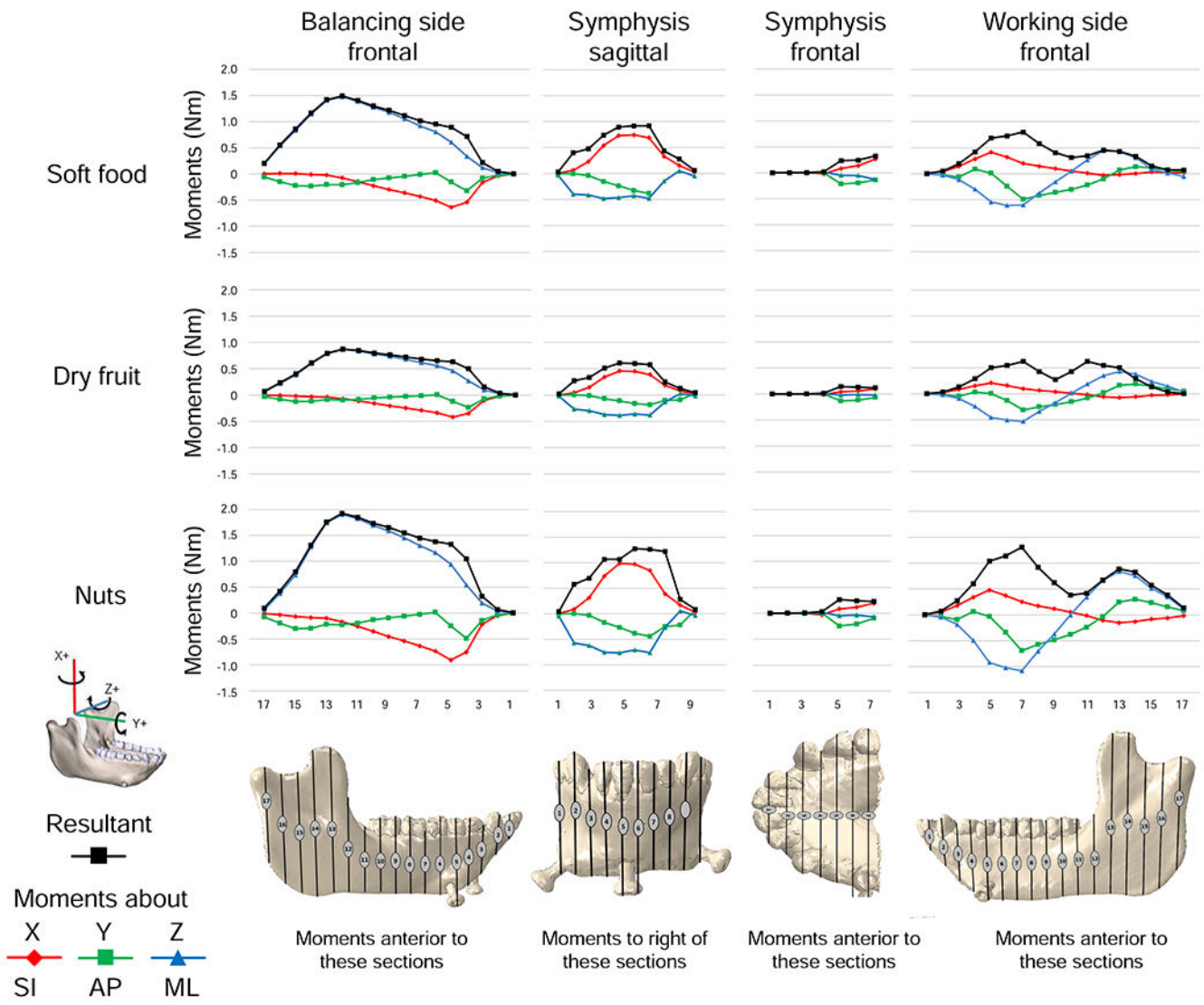

Figure 4.

Deformation and strain regimes in the balancing-side corpus and ramus during simulation of nut chewing. Strain scales in H and L apply to principal, axial and shear strains. A, B) Model deformation, in **p**osterior (A) and lateral (B) views. The left side is the working (biting) side, the right side is the balancing-side; the left P_3, P_4, and $M1_1$ are constrained against all displacements; the deformed model is transparent; the undeformed model is solid; deformation scale factor is 70. Red arrows connect homologous points between undeformed and deformed models, curved black arrows indicate negative AP twisting of balancing-side mandible; straight black arrows indicate lateral transverse bending. $F_{j.bal.}$, vertical component of balancing-side joint reaction force; $F_{m.bal.}$, vertical component of balancing-side muscle force; F_{bite}, vertical component of bite force. C, D) Transverse shear strain and AP twisting: positive transverse shear strain along the top of the corpus and endocondylar ridge (C) and negative transverse shear strain along the bottom of the balancing-side mandible (D) are associated with negative AP twisting. E) Maximum (ε_1) and minimum (ε_2)

principal strain regimes in lateral surface of balancing-side mandible. F) Sagittal shear forces acting along the balancing-side mandible. G) Sagittal shear strain on lateral surface of balancing-side mandible. H–L) Anteroposterior (AP) strains (I, J, K) and principal strains (H, L) associated with negative sagittal bending of balancing-side mandible. Maximum principal strain (ε_1) on the top of the balancing-side mandible (in H) is primarily due to AP tensile strain (in I). Minimum principal strains (ε_2) in base of mandible (in L) are primarily due to AP compressive strain (in K). The predominance of AP compressive strain in the lateral surface of the balancing-side mandible (in J) is due to lateral transverse bending of the mandible. The high values of AP compression (J, K) and of ε_2 along the lateral edge of the base of the mandible are due to superposition of lateral transverse bending and negative sagittal bending.

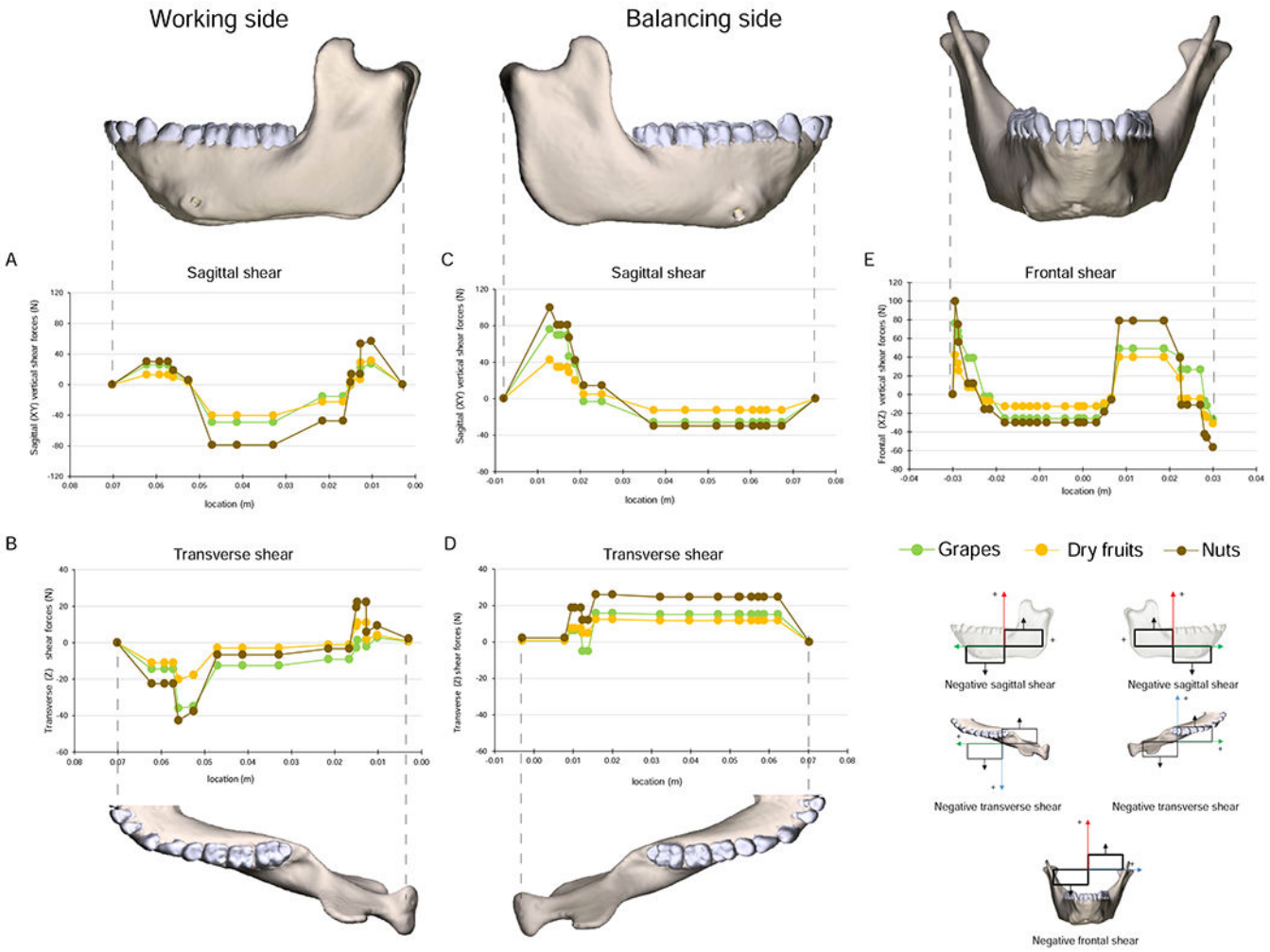

Figure 5.

Deformation and strain regimes in the working-side corpus and ramus. Strain scale in G applies to principal, axial and shear strains. A, B) Deformation regime: the left side is the working (biting) side, the right side is the balancing-side; the left P_3, P_4, and M_1 are constrained against all displacements; the deformed model is transparent; the undeformed model is solid; deformation scale factor is 70. Red arrows connect homologous points between undeformed and deformed models, curved black arrows indicate negative torsion of working-side mandible. Thick black arrows indicate vertical force components: $F_{m.bal}$ = balancing-side muscle force transmitted across the symphysis; F_{bite} = bite force; $F_{m.wk}$ = working-side muscle force; $F_{j.wk}$ = working-side joint reaction force. C, D) Transverse shear strain and AP twisting: alternating positive and negative transverse shear strain along the top (C) and bottom of the working-side corpus (D) are associated with alternating patterns of AP twisting. E) Maximum (ε_1) and minimum (ε_2) principal strain regimes in lateral surface of working-side mandible. F) Shear forces acting along the working-side mandible. G) Sagittal shear strain on lateral surface of balancing-side mandible. Sagittal shear strains are positive between the bite force and $F_{m.bal}$, negative between F_{bite} and $F_{m.wk}$, and positive between $F_{m.wk}$ and $F_{j.wk}$. H-N) Anteroposterior (AP) strains (J, K, L) and principal strains (H, I, M,

N) associated with sagittal bending of working-side mandible. Minimum principal strain (ε_2) on the top of the working-side mandible (in H) are primarily due to AP compressive strain (in J). Maximum principal strains (ε_1) in base of mandible (in M) are primarily due to AP tensile strain (in L).

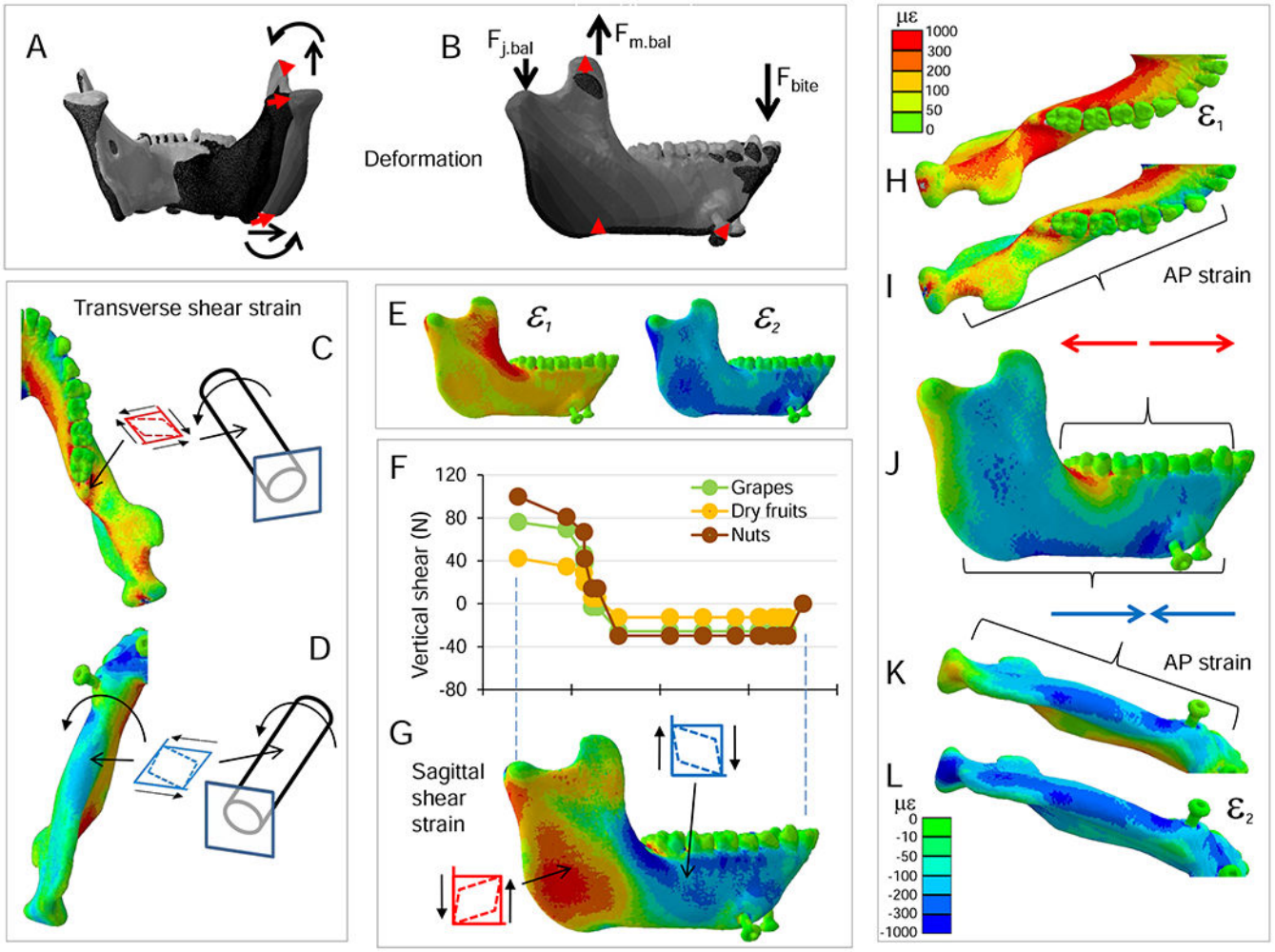

Figure 6.

Deformation and strain regimes in the symphyseal region. Scale in bottom left applies to axial and shear strains. A, E) Deformation regime. Curved arrows indicate negative torsion of both working and balancing-side corpora and rami. Straight arrows indicate lateral transverse bending of the mandible. This deformation regime includes lateral transverse bending of the balancing-side corpus and ramus, such that the balancing-side (right) condyle displaces laterally, and medial bending of the working-side corpus by transversely (to the right) directed forces transmitted by the symphysis. A-D) Posterior view. E-H) Anterior view. I, J, K) Left posterior oblique view. B, F) Maximum (ε_1) and minimum (ε_2) principal strain regimes. C) Mediolateral tensile strains are high in the lingual symphysis in association with lateral transverse bending. G) Mediolateral compressive strains on the inferior labial symphysis are associated with lateral transverse bending. D, H) Frontal (coronal) plane shear strains are opposite in sign on lingual (D) and labial (H) surfaces of the symphysis in association with negative transverse twisting. I–K) Symphyseal loading, deformation and strain regime. I) Moments based on balancing (right) side free body, representing the moments acting on the working-side of the symphysis during nut chewing (Fig. 2). The symphysis is subjected to negative transverse twisting, positive vertical twisting

(lateral transverse bending) and negative AP twisting. The transverse (J) and frontal (K) shear strain regimes are reversed on opposite faces of the symphysis due to negative transverse twisting.

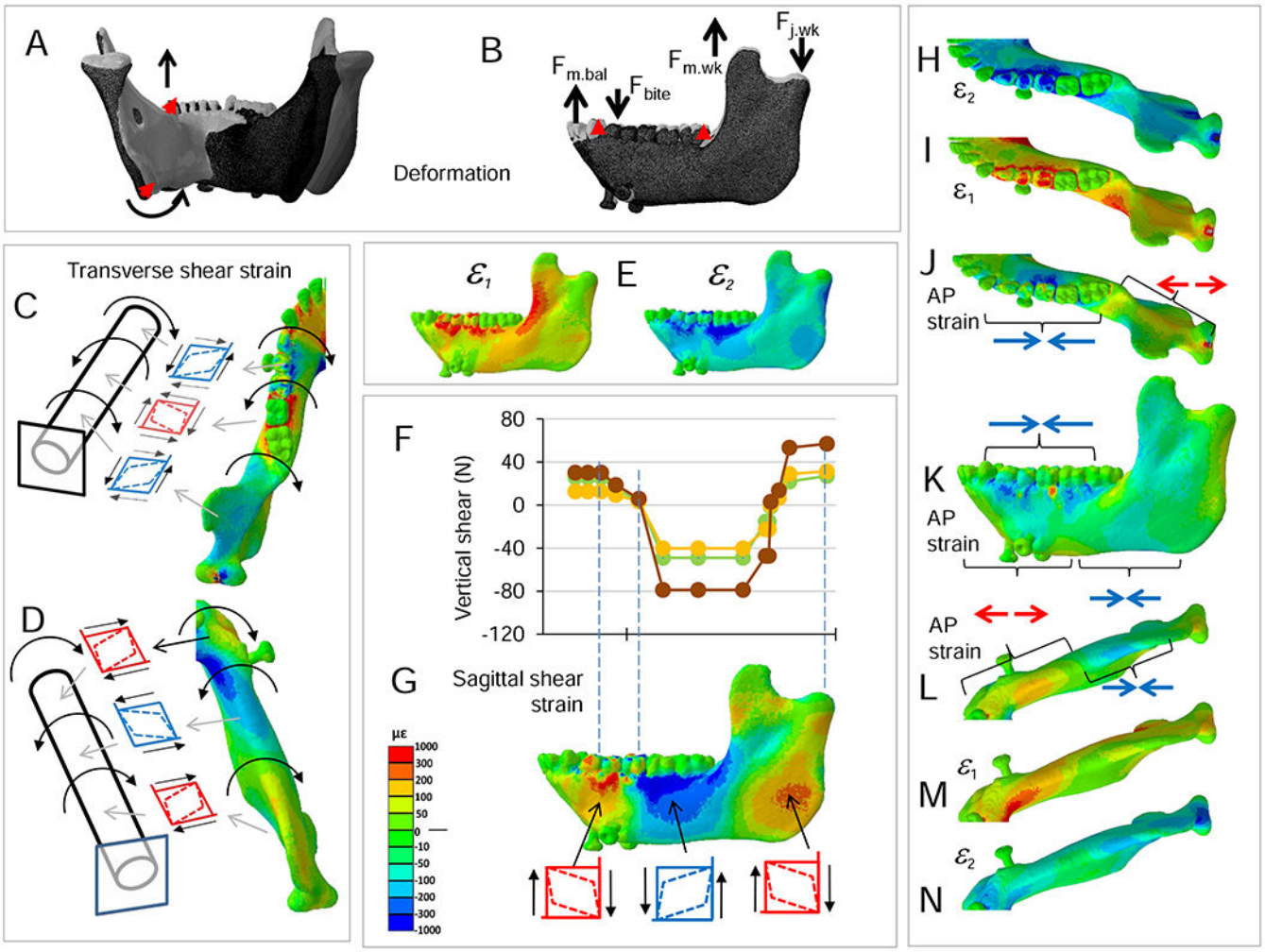

Figure 7.

Food effects on moments. Plots of differences in moments calculated as (moment during nut chewing) – (moment during grape or dried fruit chewing). All moments were of similar sign, so negative differences indicate nut chewing elicited larger negative moments and positive differences indicate nut chewing elicited larger positive moments.

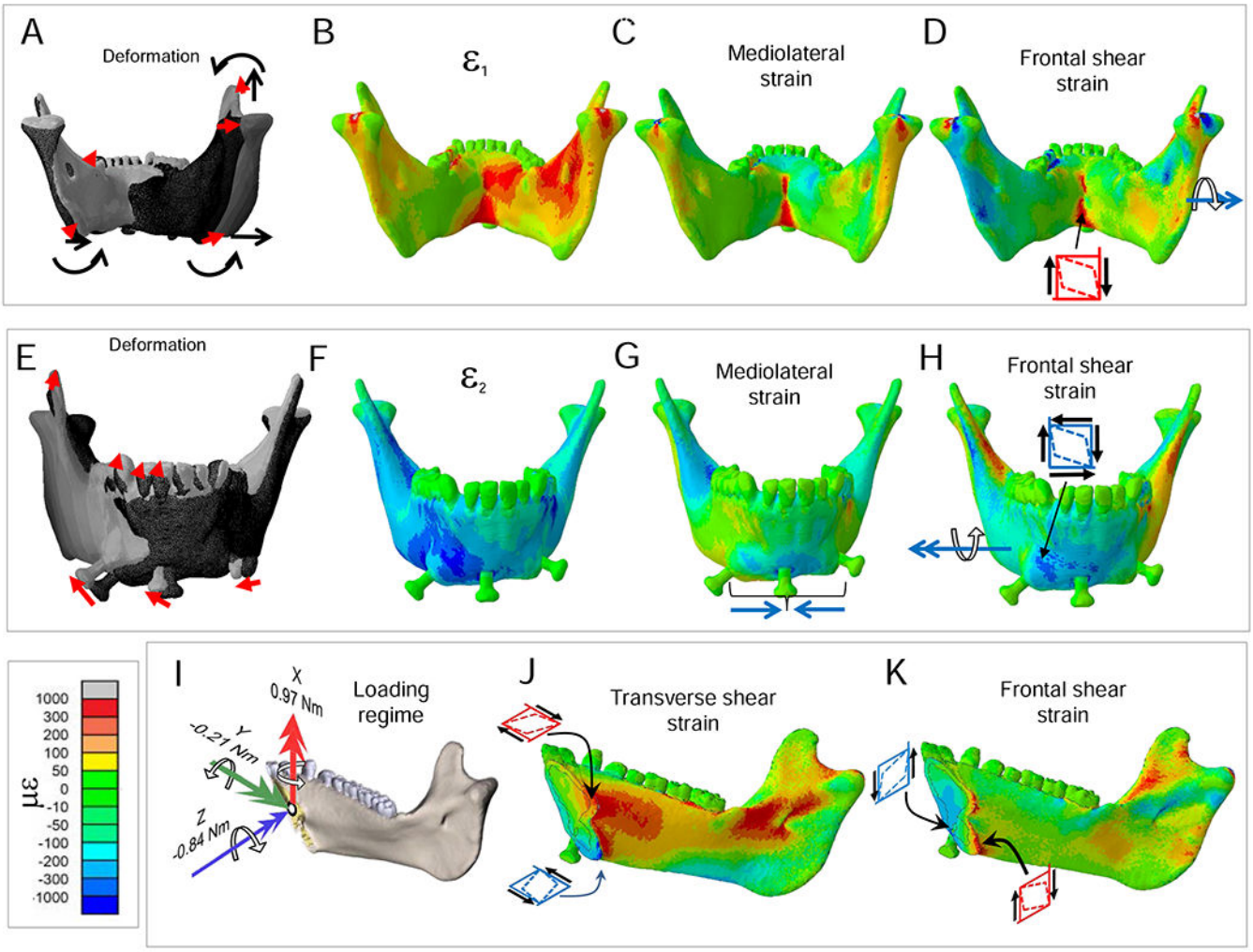

Figure 8.

Food effects on shear forces. Plots of differences in shear forces calculated as (shear during nut chewing) – (shear during grape or dried fruit chewing). All shear forces were of similar sign, so negative differences indicate nut chewing elicited larger negative shear and positive differences indicate nut chewing elicited larger positive shear.

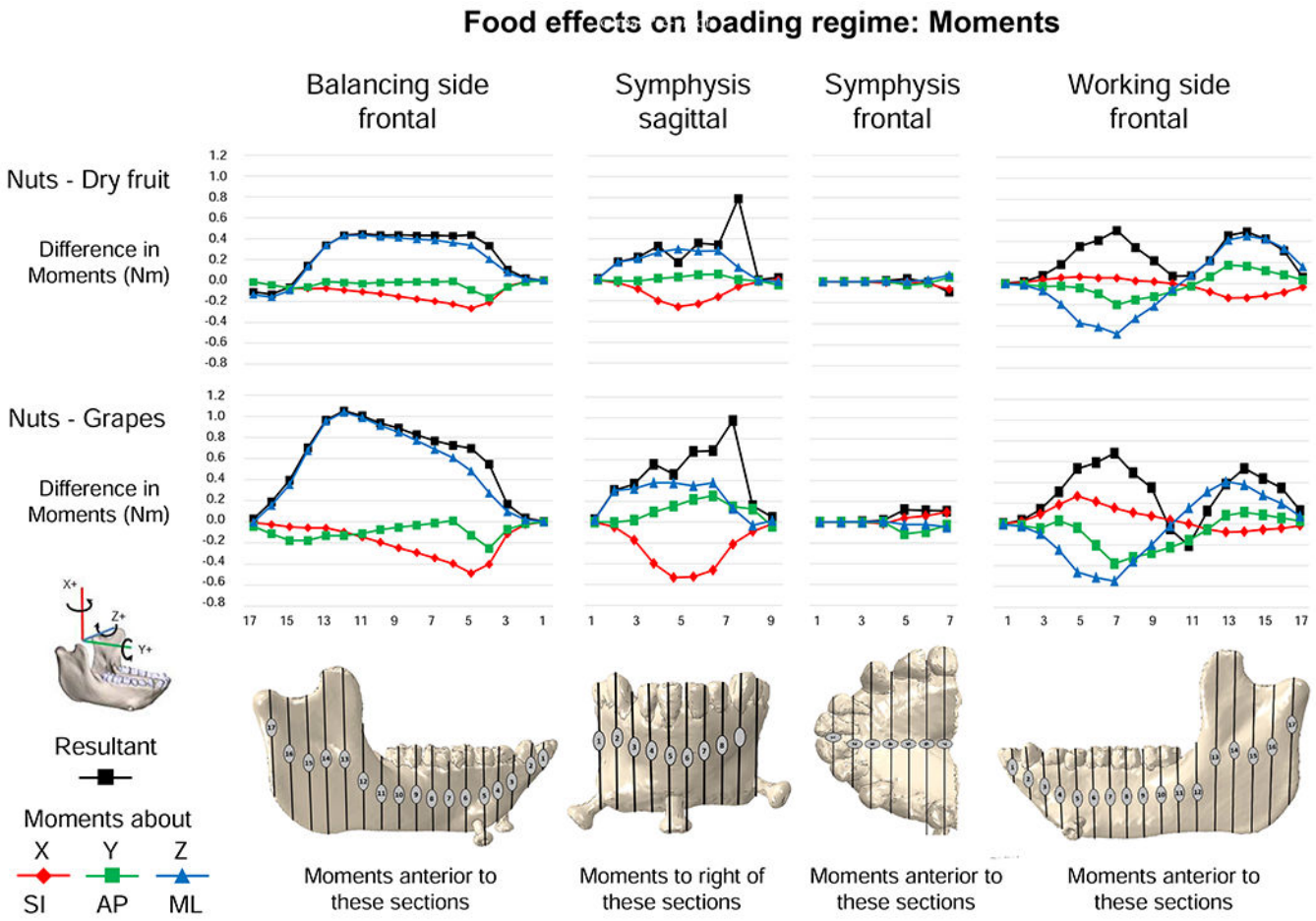

Figure 9.

Comparisons of magnitudes of strain components from simulations of mastication of nuts and dried fruit. Scale applies to all figures (principal, axial and shear strains). Figures map the distribution of differences in principal and shear strains recorded on the surfaces of the model during simulation of the power stroke of mastication on nuts and dried fruit. The top two rows present principal strains; the bottom three rows shear strains. For principal strains, the comparisons are calculated as differences in absolute values (i.e., magnitudes) for ε_1 and ε_2. For example, comparison of nut and dried fruit strain magnitudes reveals that along the endocondylar ridge ε_1 magnitudes were ca. 300 με greater during nut chewing (A–D), and along the back edge of the ramus, ε_2 magnitudes were ca. 300 με greater during nut chewing (E–H). For shear strain comparisons, the differences are direct comparisons calculated as (nut strain) - (fruit strain). The scale bar at the bottom indicates the difference in microstrain (με) between the two simulations.

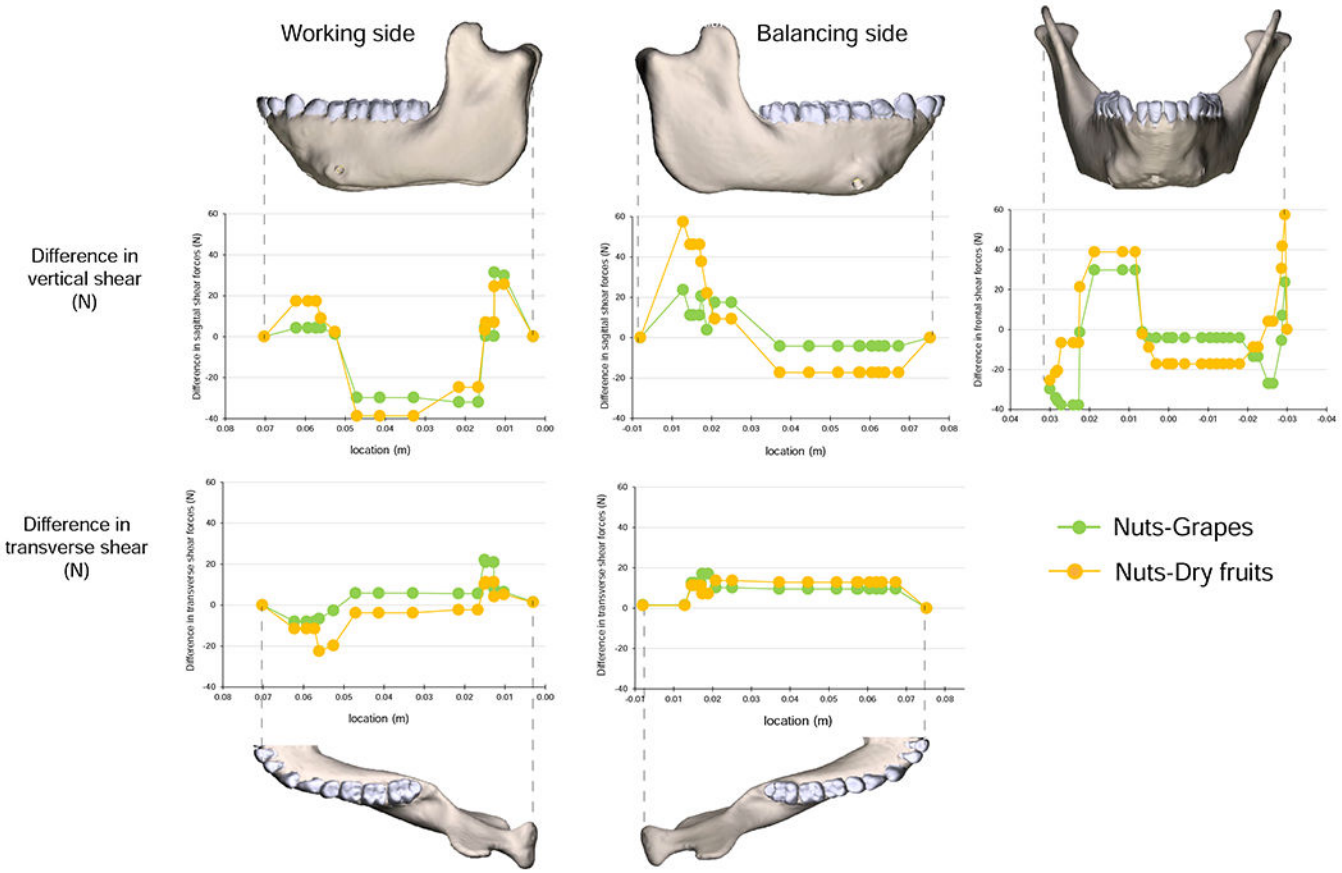

Figure 10.

Comparisons of maximum differences in magnitudes of strain components from simulations of mastication of all food types. Figures map the distribution of the maximum differences in principal and shear strains recorded on the surfaces of the model during simulation of the power stroke of mastication on any of the three foods. The top two rows present principal strains; the bottom three rows shear strains. The scale bar at the bottom indicates the difference in microstrain (με).

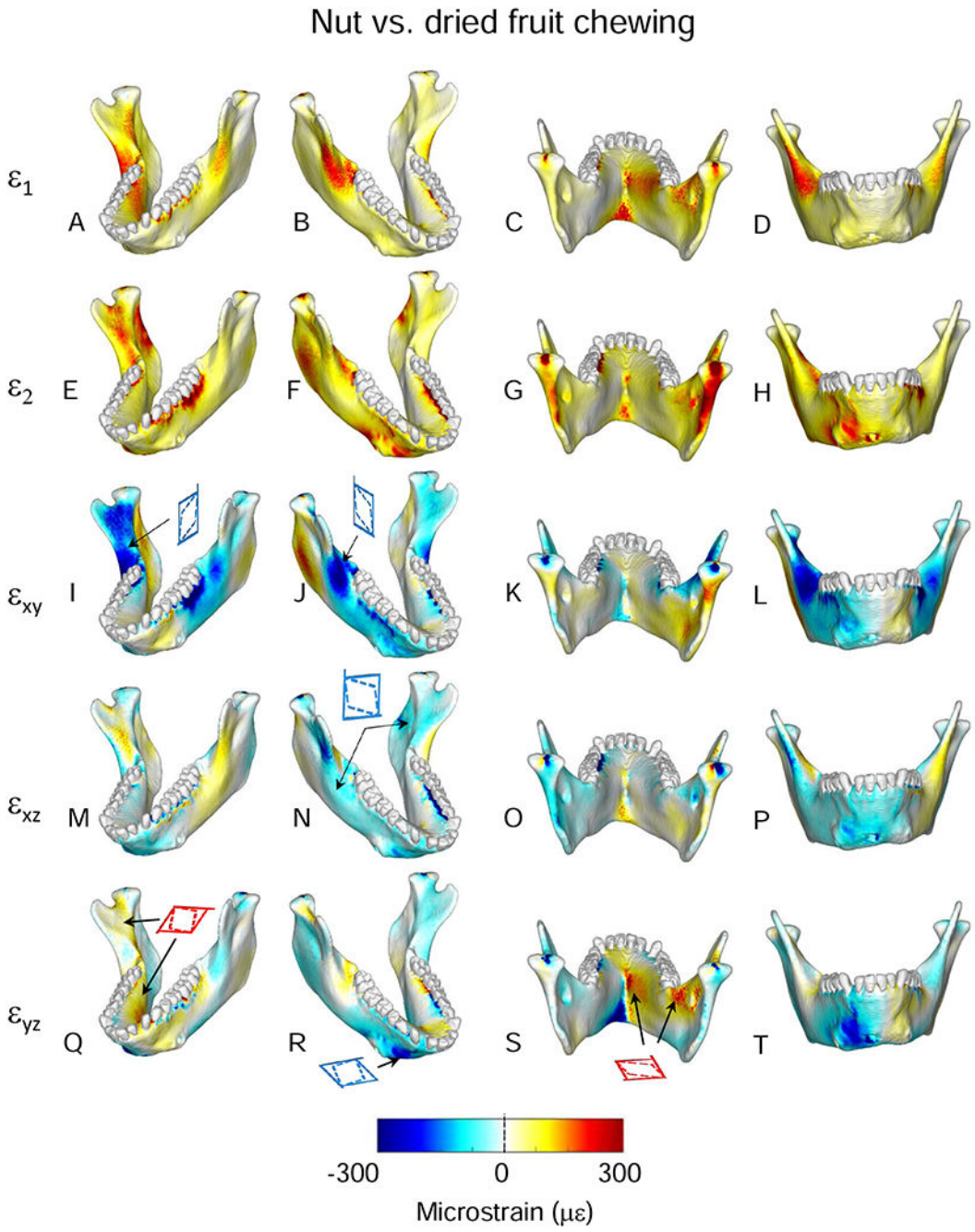

Figure 11.

Comparisons of differences in orientation of principal strains from simulations of mastication of the three food types. Figures map the distribution of the differences in principal strain orientations recorded on the surfaces of the model during simulation of the power stroke of mastication on nuts and dried fruit. The scale bar at the bottom indicates the difference in degrees. Histogram shows number of elements with given differences in principal strain orientations.

Table 1

Loading regime. Forces and force components (N) acting on the model during simulation of the power stroke on three food types.

	Grapes				Dry fruits				Nuts			
Muscle forces	**Total**	**x**	**y**	**z**	**Total**	**x**	**y**	**z**	**Total**	**x**	**y**	**z**
Anterior temporalis												
Left	35.2	33.63	−9.90	3.50	18.3	17.46	−5.14	1.82	32.9	31.45	−9.26	3.27
Right	23.2	22.61	−5.32	0.71	18.2	17.72	−4.17	0.55	45.5	44.23	−10.41	1.38
Posterior temporalis												
Left	33.9	14.81	−16.83	4.16	10.3	6.72	−7.64	1.89	16.2	10.53	−11.97	2.96
Right	33.6	8.08	−9.29	−0.76	14.0	9.14	−10.51	−0.86	37.8	24.76	−28.47	−2.34
Superficial masseter												
Left	33.1	13.93	8.58	6.29	28.2	22.45	13.82	10.13	63.4	50.41	31.03	22.76
Right	32.7	41.14	14.47	−20.91	17.3	14.79	5.20	−7.53	32.4	27.62	9.70	−14.06
Deep masseter												
Left	17.9	5.09	−0.96	4.87	3.4	2.46	−0.47	2.35	4.9	3.54	−0.67	3.38
Right	19.7	6.49	−0.41	−5.62	10.3	7.78	−0.52	−6.77	25.2	19.04	−1.28	−16.57
Medial pterygoid												
Left	27.6	8.44	1.79	−3.49	24.4	22.17	4.69	−9.17	43.7	39.65	8.38	−16.41
Right	29.0	23.55	4.42	11.32	6.4	5.72	1.07	2.75	15.9	14.13	2.65	6.79
Reaction forces												
Left condyle		−26.77	10.24	−2.10		−31.14	3.34	−3.33		−56.61	1.45	−7.08
Right condyle		−75.95	−1.20	0.00		−42.35	3.95	0.00		−99.67	18.31	0.00
Left M_1		−53.59	−2.98	22.38		−43.52	−6.32	14.90		−84.62	−13.92	30.85
Left P_4		−9.67	2.77	1.06		−6.12	0.07	2.34		−12.81	−0.42	5.12
Left P_3		−11.68	4.65	−21.46		−3.22	2.62	−9.12		−11.49	4.86	−20.17

Table 2

Moments (N m) acting anterior a section through working-side M_1.[a]

	Fx*dz	Fz*dx
Left anterior temporalis	0	0
Right anterior temporalis	−1.59	0.03
Left posterior temporalis	0	0
Right posterior temporalis	−0.91	−0.07
Left superficial masseter	0	0
Right superficial masseter	−0.90	−0.022
Left deep masseter	0	0
Right deep masseter	−0.69	−0.30
Left medial pterygoid	0	0
Right medial pterygoid	−0.41	0.01
Left condyle	0	0
Right condyle	3.62	0 (unconstrained in z)
Left M_1	−0.44	0.45
Left P4	−0.06	0.07
Left P3	−0.05	−0.31
Summed torques	Total Fx*dz = −1.44 Nm	Total Fz*dx = −0.13 Nm
Total torque	My = (Fx*dz) – (Fz*dx) = −1.31 Nm	

Abbreviations: Fx = forces in X direction (vertical, positive is up); Fz = forces acting in Z direction (medial-lateral, positive is to animal left); dX= vertical distance between section centroid and muscle attachment or reaction force centroid; dZ = medial-lateral distance between section centroid and muscle attachment or reaction force centroid; My = moments about Y-axis through m_1 centroid.

[a]Entries are equal to 0 when they are moments acting on the mandible behind the section of interest (working-side m_1). Fz is 0 at 10 the balancing-side condyle because the condyle is unconstrained in Z, so Fz*dz is 0.